A *Mycobacterium tuberculosis* secreted virulence factor disrupts host snRNP biogenesis

Komal Chauhan[1], Nishat Passricha[1], Yogita Kapoor[2], Dipanwita Datta[1], Naresh Arora[1], Mrinmoy Das[1], Kavya Rao[1], Lakshyaveer Singh[1], Ravi Dutt[1], Raman Deep Sharma[1], Binayak Sarkar[3], Basanti Malakkar[3], Haroon Kalam[1], Prince Saini[4], Lalita Mehra[5], Prasenjit Das[5], Vineet Ahuja[6], Amit Singhal[7,8], Vinay Nandicoori[2, 3] and Dhiraj Kumar[1]*

[1]Cellular Immunology Group, International Centre for Genetic Engineering and Biotechnology, Aruna Asaf Ali Marg, New Delhi-110067, India
[2]Centre for Cellular and Molecular Biology, Hyderabad, India
[3]National Institute of Immunology, Aruna Asaf Ali Marg, New Delhi-110067, India
[4]Department of Biological Sciences, Indian Institute of Science Education and Research Mohali, Punjab 140306, India
[5]Department of Pathology, All India Institute of Medical Sciences, New Delhi-110012, India
[6]Department of Gastroenterology, All India Institute of Medical Sciences, New Delhi-110012, India
[7]A*STAR Infectious Diseases Labs (A*STAR ID labs), Agency for Science, Technology and Research (A*STAR), Singapore, Singapore.
[8]Singapore Immunology Network (SIgN), A*STAR, Singapore, Singapore.

Running title: Regulation of host RNA splicing by Mtb

*Correspondence- dhiraj@icgeb.res.in

Abstract

We earlier reported that *Mycobacterium tuberculosis* (*Mtb*) alters host RNA splicing to help its intracellular growth. Here, we report an unprecedented mechanism whereby a secreted virulence factor from *Mtb* interferes with the biogenesis of key spliceosomal components, causing an altered RNA splicing pattern. A high-throughput yeast-2-hybrid screen identified several *Mtb*-secreted proteins that can interact with the host RNA splicing factors (SFs). Through custom-designed in-cell assays, we show that one of those proteins, Rv1435c, targets specific exon-skipping events to alter RNA splicing. We show that Rv14345c or **h**ost **s**plicing **r**egulator 1 (hsr1) facilitates direct interaction between *Mtb* phagosomes and U5 snRNA and SNRPF, key components of the snRNPs. Genetic deletion of *hsr1* reverses the specific exon-skipping events caused by WT *Mtb* infection. The *Δhsr1* strain shows compromised growth during *ex vivo* infection in the macrophages and *in vivo* infection in the mice. Tissue sections from the WT *Mtb* or *Δhsr1*-infected mice showed significant hsr1-dependent SNRPF staining, a phenomenon also noted in the human intestinal tuberculosis (ITB) biopsies. We infer that hsr1 is a virulence factor which alters RNA splicing by interacting with U5snRNA and SNRPF. The splicing regulators from the host and pathogen are novel targets for anti-tuberculosis therapy.

54 **Introduction**

55 Tuberculosis (TB) caused by the bacterial pathogen *Mycobacterium tuberculosis* (*Mtb*) is a
56 considerable challenge to the global sustainable development goals on health. With more than
57 10 million new TB cases and nearly 1 million deaths globally, the conventional approaches
58 for prevention and control are increasingly looking insufficient to eradicate TB. The
59 emerging paradigm on novel TB therapy envisages exploiting host-directed therapy (HDT).
60 The advantage of HDT is its perceived universality in targeting drug-resistant or drug-
61 sensitive infections. Also, HDTs, combined with antibiotics, are expected to hinder the
62 development of new drug-resistant strains. Over the past two decades, several studies
63 identified and reported host-dependency factors that help the intracellular growth and
64 survival of *Mtb*, mostly by modulating the anti-bacterial functions of the hosts [1-7]. In a
65 genome-wide analysis of identifying such host factors, proteins from diverse functional
66 classes, including gene expression, were reported to have pro-bacterial functions [6].
67
68 The transcriptional response of the host cells to *Mtb* infections has been studied extensively[8-
69 12]. While the immediate response of host cells following infection with *Mtb* involves
70 processes like trafficking, signalling and metabolic alterations, the long-term shaping of host
71 response is decided by reshaping the transcriptional landscape of the cells[13,14]. Eukaryotic
72 gene expression involves several post-transcriptional regulatory events, including capping,
73 poly-adenylation, RNA splicing, etc. We previously showed that in the *Mtb*-infected
74 macrophages, several genes classically known for their anti-bacterial functions were spliced
75 in a manner that did not allow their translation or the polypeptides thus formed were
76 truncated[13]. Moreover, the alternatively spliced transcripts often lacked critical functional
77 domains due to exon exclusion events[14,15]. Several other studies together converge to the
78 notion that RNA splicing could be a central vulnerability for the pathogens to exploit.
79
80 However, the molecular mechanism that allows pathogens, including *Mtb*, to alter host RNA
81 splicing in a targeted manner remains poorly understood. RNA splicing is an evolutionarily
82 conserved mechanism among eukaryotes and involves the assembly of a large multi-
83 molecular complex called spliceosome at the exon-intro junctions[16-22]. The key components
84 of the spliceosomes are small nuclear ribonuclear proteins or snRNPs, comprising snRNA
85 and associated proteins[23-31]. Interestingly, snRNPs are formed through complex protein-RNA
86 interactions spanning across the nucleus and the cytosol[29,32]. In addition, accessory proteins
87 like hnRNPs, SR proteins and SRSF proteins play an important role in recognizing the exon-

88 intron junctions and splicing reactions[17,19,33,34]. Cumulatively, there are plenty of potential
89 steps where secreted virulence proteins from *Mtb* could intercept the RNA splicing
90 machinery, thereby altering the course of downstream reactions. Secreted virulence factors of
91 *Mtb* are classically known to interfere with cytosolic events like trafficking, antigen
92 presentation, bioenergetics and nuclear events like epigenetic regulations [35-39].
93
94 To understand how *Mtb* alters host RNA splicing, we hypothesized that certain secreted
95 virulence factors of *Mtb* could interact with and alter the assembly and/or recognition of
96 spliceosome complexes or their components. Here, through a high throughput yeast-2-hybrid
97 screening between secreted *Mtb* proteins and host splicing-related proteins or splicing factors
98 (SFs), we identify several interacting partners between the two. We rationally narrowed it
99 down to one *Mtb* protein, Rv1435c, to understand the molecular mechanism in detail. Using a
100 genetic knockout of Rv1435c, we show that cytosolic interactions with snRNP biogenesis
101 components allowed *Mtb* to alter the stoichiometry of snRNPs in the cells, eventually altering
102 the RNA splicing process.
103

Results

Dysregulated spliceosome complex composition in *Mtb*-infected macrophages

Previously, we reported a targeted alteration of host RNA splicing pattern upon *Mtb* infection in the macrophages[13]. We also showed how altered RNA splicing impacted cellular function since a lot of target genes were spliced in a manner that led to the mRNAs, which were either non-functional (lacking specific functional domains), unstable or could not get translated (Fig. 1A)[14] . These alterations were reported as advantageous for the pathogen inside the host macrophages. To understand how RNA splicing was specifically altered in the infected macrophages, we systematically analyzed the RNA splicing process in these cells. RNA splicing requires the assembly of a large multimolecular complex, called the spliceosome, in a step-wise manner, which helps in the recognition, excision of the introns and stitching of the exons together (Fig. 1B). To analyze the assembly of spliceosome complexes in the *Mtb* infected macrophages, we decided to purify and analyze the *in vivo* assembled spliceosome complexes from these cells. THP-1 macrophages were infected with H37Rv (the laboratory strain of *Mtb*) at 1:10 MOI, and at 48 hours post-infection (h.p.i.), cytosolic and nuclear extracts were prepared without disrupting the assembled spliceosome complexes (see methods). The spliceosome complexes were then immunoprecipitated using the anti-SNRPB antibody (Y-12) followed by mass spectrometry analysis (Fig. 1C). The detailed list of identified peptides and proteins is shown in Table S1. The quantitative analysis of spliceosome-related proteins is shown as the heatmap in Fig. 1D. Several host splicing proteins showed distinct levels and nucleo-cytoplasmic distribution in the *Mtb*-infected macrophages compared to the uninfected cells (Fig. 1D). Thus, proteins like RPL4, SF3B2 and SYNCRIP showed contrasting nucleo-cytoplasmic distribution in the infected cells (Fig. 1D). In contrast, proteins like SNRNPs and HNRNPs showed severe depletion of the nuclear pool in the infected macrophages (Fig. 1D). The SNRNP proteins were particularly intriguing since they are critical for the assembly of small nuclear ribonuclear proteins (snRNPs)[23,26,40,41]. Dysregulation of these SFs suggests a systemic perturbation of the splicing machinery in *Mtb*-infected macrophages.

Identification of *Mtb* proteins that could interact with host spliceosome complex proteins

Since a large number of spliceosome-associated proteins were dysregulated, we hypothesized that the virulent factors secreted by *Mtb* in the infected macrophages could likely be interacting with some of these proteins and responsible for their dysregulation. To test this

138 hypothesis, we decided to screen whether any secreted protein from *Mtb* could interact with
139 the components of host RNA splicing machinery using the yeast-2-hybrid (Y2H) method.
140 The *Mtb* genes encoding the secreted proteins were part of the bait library (binding domain or
141 BD vector), while the human spliceosome-associated proteins encoding genes constituted the
142 prey library (activation domain or AD vector). In total, we had 384 *Mtb* genes in the BD
143 library, including 37 negative controls (Table S2). For the secreted protein list, we relied
144 mainly on our recent secretome study[42] in addition to other *Mtb* secretome studies[36,43-45]
145 (Table S2). The AD library was comprised of the protein-coding isoforms of genes belonging
146 to functional classes "RNA splicing" and "Spliceosome function" (~162 clones), making it a
147 unique custom library of human transcripts (Table S2). In the BD library, we also included a
148 few negative controls (proteins which are never reported in the secretome analysis, Table S3).
149 Four independent mating reactions between 384 BD clones and 162 AD clones, amounting to
150 about 2,48,832, were conducted to obtain the interaction. The schematic for the Y2H assay is
151 shown in Fig. 2A. In total, 123 Mtb proteins showed interactions with one or more SFs,
152 together consisting of 439 incidences of interactions (Table S4). Out of these 439, 121
153 interactions were a result of autoactivation (Table S4). The BD clones showing autoactivation
154 were excluded from the list of interacting proteins. A few negative control list clones also
155 showed interactions, including 56 autoactivation incidences (Table S3). The interacting BD
156 clones that did not show autoactivation were considered true interactors and mapped as a
157 network to represent the *Mtb*-host spliceosome interactome, comprising 54 human SFs and
158 117 *Mtb* proteins (Fig. 2B, Table S5).
159 The interactions spanned across all classes of host proteins that regulate RNA splicing,
160 including RNA polymerases, Sm proteins, SMN complex proteins, U2 snRNP proteins, LSm
161 proteins, U4/U5.U6 tricomplex proteins and non-snRNP proteins (Fig. 2C). The Venn
162 diagram in Fig. 2C shows number of *Mtb* proteins interacting with proteins from each of
163 these classes discussed above. Overall, host proteins from RNA Pol II subunits, Sm core,
164 catalytic step II factors, HnRNPs and SMN complex and *Mtb* proteins from information
165 pathway, virulence factors and conserved hypothetical proteins functional classes showed
166 maximum interactions (Fig. S1A). Interestingly, host proteins from similar functional steps in
167 RNA splicing shared their interacting partners from the *Mtb* (Fig. 2D). The Mtb proteins
168 showing interaction also represented diverse functional classes (Fig. S1B).
169 Finally, due to the inclusion of protein-coding splice variants of host SFs in the AD library,
170 eighteen genes were represented by more than one transcript in the interactions list (Fig. S2).
171 Out of those, POLR2H, SYF2, SNRPD2, LSm7, RBMX, LUC7L2, DCAF4, PPIH and

172 U2AF1 showed interactions with the *Mtb* proteins (Fig. S2). Curiously, the spliced variants
173 with a truncated coding region interacted with many *Mtb* proteins compared to their full-
174 length counterparts (Fig. S2). While this observation suggests looking at protein homeostasis
175 in the *Mtb*-infected macrophages more carefully, we decided to remain focused on our
176 objective of understanding the mechanism of infection-induced alternative splicing.
177
178 ***Mtb* secretory protein Rv1435c could alter host RNA splicing**
179 Several *Mtb* secretory proteins showed promising interactions in the Y2H assays above.
180 Before taking any of these proteins for further mechanistic explorations, it was important to
181 verify them on two accounts- one, if the identified *Mtb* secreted protein could alter host RNA
182 splicing and two, whether the identified interacting partners in the Y2H assay also interacted
183 with each other in a mammalian system. We picked up a few *Mtb* proteins, one showing a
184 very high number of interactors (Rv1643, 22 interactions), another with an intermediate
185 number of interactors (Rv1566c, 13 interactors) and a third with a low number of interactors
186 (Rv1435c, 5 interactors) (Table S3). To test whether these *Mtb* proteins could alter host RNA
187 splicing in a targeted manner, we first developed a few assays. For the functional assays, it
188 was critical to choose target genes for which splicing events were to be measured. We chose
189 around five target genes from the host, including *ACSL1*, *ACADVL*, *DDX11*, *DDX42* and
190 *NFYA*, which consistently showed exon exclusion events upon *Mtb* infection[13]. We designed
191 primers to score for the test exon exclusion event, exon inclusion event, and a set of primers
192 from the exon junctions (Fig. S3A). The exon exclusion primers clearly showed, upon *Mtb*
193 infection, an increase in the expression of selected transcripts of the genes where the test exon
194 was excluded (Fig. S3B). On the contrary, with the exon inclusion primers, except for the
195 *ACSL1* transcript, others either did not show any regulation (ACADVL and DDX42) or
196 showed a decrease in expression upon *Mtb* infection (DDX11 and NFYA) (Fig. S3C).
197 Finally, primers designed from the junction of exons 1 and 3 conclusively showed that the
198 selected transcripts showed clear cases of *Mtb* infection-induced exon exclusion (Fig. S3D).
199 Next, we used a splicing reporter assay, which included a constitutive reporter construct
200 *pRint* and a test construct *pGint* [46] (Fig. 3A). The *pGint* reporter construct was modified to
201 include the test exon (middle exon) along with the flanking 100bp intronic sequences (Fig.
202 3A). The HEK293T cells stably expressing *pRint* were transfected with *pGint_ACADVL,*
203 *pGint_ACSL1, pGint_DDX11, pGint_DDX42* and *pGint_NFYA* along with either a control
204 non-interacting *Mtb* protein encoding plasmid (NIC) or plasmid encoding for *Rv1435c,*
205 *Rv1566c or Rv1643* (Fig. 3B). Expressing NIC alone led to a marginal but consistent increase

206 in the %pGint^{+} cells in the case of *DDX11* and *ACSL1* (Fig. 3C). Rv1435c and Rv1566c
207 showed a significant increase in %pGint^{+} cells in the case of all except *ACSL1* over and
208 above corresponding NIC expression (Fig. 3C). Unlike Rv1566c and Rv1435c, for Rv1643,
209 significant increase compared to the NIC were noted in the case *ACADVL*, *DDX11* and
210 *DDX42* but not in the case of *NFYA* (Fig. 3C). Despite the limitation that we used only a
211 handful of target RNA splicing, we could show that the three selected *Mtb* proteins were able
212 to alter host RNA splicing.
213 In the above assay, among the three *Mtb* proteins analyzed, *Rv1566c* and *Rv1435c* showed a
214 stronger influence on exon exclusion events. Among the two, Rv1435c also contains a
215 signalP, which is essential for secretion through the classical bacterial secretory pathway [43,44].
216 Secondly, while some function for Rv1566c was assigned earlier [45,47], Rv1435c remains an
217 uncharacterised protein. Therefore, we decided to pursue further characterization of Rv1435c
218 in regulating host RNA splicing events.
219 First, we verified the physical interactions between Rv1435c and its Y2H counterparts from
220 the human SFs. Out of five interacting SFs, we picked up two Rv1435c interacting SFs,
221 GEMIN3 or DDX20 and PRPF18, to verify interactions in the mammalian cells. Flag-tagged
222 *Rv1435c* was co-expressed along with HA-tagged human counterparts in HEK293T cells,
223 followed by co-immunoprecipitation. Consistent with the results from the Y2H screen, both
224 anti-Flag and anti-HA pulldowns were able to co-immunoprecipitate each other, suggesting
225 strong interaction of Rv1435c protein with the two human proteins GEMIN3 and PRPF18
226 (Fig. 3D). Therefore, Rv1435c was able to induce exon exclusion event in the *in-cell* reporter
227 assay and also showed physical interaction with human SFs in the mammalian cells.
228
229 **A surrogate infection model using *M smegmatis* knock-in line shows a direct role of**
230 **Rv1435c in altering host RNA splicing during infection**
231 Next, to test whether Rv1435c could also impact these exon exclusion events during
232 infection, we used the non-pathogenic *Mycobacterium smegmatis* (*Msmeg*) strain. We cloned
233 Rv1435c under a Tet-inducible promoter and expressed it in the *Msmeg*, making it
234 *Msmeg::Rv1435c* (Fig. 3D). We confirmed that Rv1435c was expressed and secreted by the
235 modified *Msmeg* upon induction (Fig. S4A). Next, we infected THP-1 macrophages with
236 *Msmeg, Msmeg::vector or Msmeg::Rv1435c,* which were either untreated or treated with
237 ATC before infecting the cells (Fig. 3D). Specific exon exclusion events were then tested
238 using RT-PCR assays against all the five target events described above. For *ACADVL*,
239 *DDX42*, *ACSL1* and *NFYA*, while we did observe a trend, the increase in exon exclusion

event when *Msmeg::Rv1435c* line was induced by anhydrotetracycline (ATC), it was not very consistent and significant (Fig. S4B). In the case of DDX11, infection with *Msmeg* alone, *Msmeg::vector* or *Msmeg::Rv1435c* did not induce the exon exclusion event (Fig. 3E). However, when *Msmeg::Rv1435c* was induced overnight with ATC, there was a significant increase in the case of *DDX11* exon exclusion event (Fig. 3E). Overall, results from the above sections show that Rv1435c from *Mtb* interacts with select host SFs and also alters specific host RNA splicing events.

Mtb Rv1435c is a secretory protein with no assigned function

Once the role of Rv1435c in altering host RNA splicing was verified, we were curious to know what was known about this protein or its homologues from other species. The *Mtb* Rv1435c is a 202 amino acid-long polypeptide; a Pfam search revealed the presence of signalsP (1-33) at the N-terminal, indicating its secretion through the classic sec-mediated pathway (Fig. S4C). The remaining polypeptide segment (34-171) is classified as an extracytoplasmic region with a disordered region towards the C-terminal (172-202, Fig. S4C). Similar structural features were also revealed by AlphaFold Protein Structure Database[48] (Fig. S4D). Sequence search revealed the presence of its orthologues in several pathogenic and non-pathogenic species of the genus *Mycobacterium* (Fig. S4E). Classifying these orthologues through a dendrogram analysis revealed an interesting pattern. In truly pathogenic species like *Mtb* and *M. marinum*, this gene is classified as a secreted protein with no function assigned (Fig. S4F). In opportunistic pathogenic species, like *M. helveticum, M. paratuberculosis, M. shinjukuense* and a few other unclassified species, this gene has been assigned the function of secreted beta-xylosidase (Fig. S4F). Even in a few truly pathogenic species like *M. lacus* and *M. heildelbergense*, this gene is characterized as secreted beta-xylosidase. It is possible that altering RNA splicing through interaction with the host spliceosome complex emerged as a function during the evolution of the pathogenic species.

MtbΔRv1435c fails to alter target gene alternative splicing during infection

Next, to establish that Rv1435c could be directly involved in altering the host RNA splicing during *Mtb* infection, we deleted the *Rv1435c* gene in *Mtb* using recombineering[49] to generate the knockout strain *MtbΔRv1435c* (Fig. 4A). The knockout (KO) of *Rv1435c* was verified by PCR using specific primers as described in the methods and also by RT-PCR to test the expression of Rv1435c RNA in the KO cells (Fig. 4B and 4C). We also generated an

273 *Rv1435c* complemented strain by electroporating the WT *Rv1435c* encoding plasmid in the
274 *MtbΔRv1435c* cells to generate *MtbΔRv1435c::WT*. Next, we infected THP-1 macrophages
275 with the WT *Mtb*, *MtbΔRv1435c or MtbΔRv1435c::WT* and assayed for the exon exclusion
276 events in the five target genes, as described earlier. While the WT *Mtb* infection, expectedly,
277 increased the exon exclusion event for each of the five target genes, in *MtbΔRv1435c*-
278 infected THP-1 macrophages, the exon exclusion events were significantly downregulated
279 (Fig. 4C). In the THP-1 macrophages infected with *MtbΔRv1435c::WT*, the exon exclusion
280 event was restored to the levels observed during WT *Mtb* infection (Fig. 4C). These results
281 indicate that Rv1435c protein of *Mtb* can alter the targeted host RNA splicing events in the
282 infected macrophages and therefore, we named it as **h**ost **s**plicing **r**egulator 1 or hsr1.
283
284 ***Mtb* hsr1 binds to and sequesters U5snRNA in the cytosol**
285 Next, we wanted to understand the mechanism of hsr1-mediated alteration in host RNA
286 splicing. In the spliceosome complex pulldown results (Fig. 1) and the Y2H screening results
287 (Fig. 2), several proteins from the snRNP complexes were present. This included proteins
288 from the SMN complex like GEMINs, DDX proteins and those from the heptameric core that
289 are recruited to the 3' sm Site of snRNAs for the biogenesis of snRNPs. The biogenesis of
290 snRNPs follows an evolutionarily conserved nucleo-cytoplasmic shuttling, where snRNAs,
291 upon being synthesized in the nucleus, are exported to the cytosol (Fig. 5A). In the cytosol,
292 snRNAs bind with the SMN complex, followed by the recruitment of sm Core proteins[50]
293 (Fig. 5A). We anticipated that snRNP biogenesis, due to its cytosolic trajectory, could be a
294 potential target of *Mtb* proteins-mediated alteration. We analyzed the levels of two snRNAs-
295 U2 and U5 snRNAs, in the *Mtb*-infected macrophages using Fluorescence In Situ
296 Hybridization (FISH). While the U2 snRNA showed no noticeable pattern (Fig. S5A), we
297 noted a significant regulation in U5 snRNA levels in *Mtb*-infected macrophages at 24 and 48
298 hpi (Fig. 5B). While there was a significant decline in U5 snRNA levels at 24 hpi, we noted a
299 significant increase in U5 snRNA levels at 48 hpi (Fig. 5B-C). To our surprise, we also
300 observed a direct interaction between *Mtb* phagosomes and U5 snRNA (Fig. 5D). The U5
301 snRNA interaction with the *Mtb* phagosomes increased over time from almost no noticeable
302 interaction at 24 hpi to significantly high interaction at 48 hpi (Fig. 5D). It appeared that *Mtb*
303 phagosomes were binding and sequestering the U5 snRNA in the cytosol (Fig. 5D). Next, to
304 test whether hsr1 was by anyway involved in this binding, we infected THP-1 macrophages
305 with WT *Mtb* or *Δhsr1* and quantified the FISH signals to compare the interaction between

306 U5 snRNA and phagosomes (Fig. 5E). We noted a significant decline in U5 snRNA
307 interaction with the phagosomes in the case of *Δhsr1* infection (Fig. 5E). The above results
308 suggest that hsr1 was responsible for binding with U5 snRNA in the cytosol. Any defect in
309 snRNP biogenesis is known to alter the global RNA splicing pattern[16,30,31,51-54] . Therefore, it
310 was likely that the altered RNA splicing events regulated by hsr1 could be due to its
311 interaction with the U5 snRNA.
312
313 **Mtb *hsr1* interacts with SNRPF, a key sm Core protein in the cytosol**
314 The hsr1-dependent interaction of *Mtb* phagosomes with U5 snRNA raised the question of
315 whether the interaction involved only the U5 snRNAs or reflected the binding of the entire
316 U5snRNP complex. The snRNP complexes, as discussed above, comprise proteins from
317 SMN complexes like GEMINs, SMNs, etc and the heptameric ring of sm Core proteins,
318 including SNRPB, SNRPD1, SNRPD2, SNRPC, SNRPF, etc. We analyzed some of the
319 marker proteins of snRNPs using confocal microscopy, including DDX23, GEMIN8,
320 GEMIN3, Lsm7, SNRPD2 and SNRPF (Fig. 6A and S6). While some of these, like DDX23,
321 GEMIN8, SNRPD2 and Lsm7, showed some random interactions with the *Mtb* phagosomes,
322 none of them showed a pattern similar to that of U5 snRNA (Fig. S6). The only protein which
323 showed U5 snRNA-like interaction with *Mtb* phagosome was SNRPF (Fig. 6A). Moreover,
324 we further verified that SNRPF interaction with *Mtb* phagosomes was also hsr1 dependent
325 since there was a sharp decline of their interaction when *Δhsr1* strain was used for infection
326 (Fig. 6B). Curiously, SNRPF was also part of our Y2H prey library; however, we did not see
327 any interaction between SNRPF and hsr1 in the Y2H assay. Since our criteria for selecting
328 positive interactions were very stringent, we sought to test whether these two proteins interact
329 in the coimmunoprecipitation assay. In the HEK293T cells overexpressing Rv1435c-FLAG
330 and SNRPF-HA, we observed that FLAG immunoprecipitation was able to pulldown
331 SNRPF-HA (Fig. 6C). However, since other smCore proteins line SNRPD2 did not show
332 noticeable interaction with *Mtb* phagosomes, we believe that Mtb phagosomes, though hsr1
333 specifically binds with U5 snRNA and SNRPF. These results suggest that *Mtb* hsr1 facilitates
334 the phagosome interaction with U5 snRNA and the smCore protein SNRPF, likely
335 contributing to an altered host RNA splicing.
336
337 ***Mtb* hsr1 secretion and, therefore, its impact on host RNA splicing is ESX1-dependent**

338 The hsr1 protein was a part of the list of *Mtb* proteins present in the culture filtrate, indicating
339 their secretion [42]. However, whether hsr1 also gets secreted during macrophage infection is
340 unknown. Secretion during infection could be a critical factor for the ability of hsr1 to
341 interact with the human spliceosome components. We generated antisera against hsr1 and
342 confirmed its specificity by immunoblotting and microscopy before using it to examine the
343 secretion of hsr1 during macrophage infection (Fig. S6A). In the uninfected macrophages,
344 expectedly, we could not see any signal for hsr1; however, in the WT *Mtb*-infected
345 macrophages, we could see several hsr1 foci on *Mtb* phagosomes and in the cytosol (Fig.
346 6D). When we used the Δ*hsr1,* there was no noticeable signal of hsr1 protein in the
347 phagosomes or in the cytosol (Fig. 6D). When we used the complemented strain Δ*hsr1::WT,*
348 the signal for hsr1 on the bacterial phagosome and in the cytosol was restored (Fig. 6D). We
349 next question, how *Mtb* hsr1 was secreted during macrophage infections. For access to
350 cytosol, the type VII secretion system ESX is critical, which is known to form pores in the
351 phagosome membrane, allowing access to the cytosol[37,45]. To test that, we used a strain
352 lacking CFP10 and ESAT6 (*ΔCE*), the two critical components of the ESX1 secretion system
353 [42,55,56]. In *ΔCE*-infected macrophages, we could not observe any signal for hsr1 in the cytosol
354 of infected cells (Fig. 6D). Moreover, even secretion of hsr1 appeared to be ESX1-dependent
355 since there was no hsr1 signal from the phagosomes (Fig. 6D). This was surprising since
356 sequence analysis predicted a putative signalP sequence at the N-terminal of hsr1, making it a
357 substrate of sec system[42]. Finally, when we used a complemented strain *ΔCE::WT*, where
358 both ESAT6 and CFP10 were restored, we could see hsr1 signal, both at the phagosomes and
359 in the cytosol (Fig. 6D). These results suggest that ESX1 pathway plays a central role in hsr1
360 secretion. The logical question next was to test whether that also impacts exon exclusion
361 events in the host target genes through alternative splicing. We compared specific exon
362 exclusion events in the case of ACADVL and ACSL1, and in both cases, *ΔCE* strain
363 infection behaved similar to *Δhsr1* infection, whereas *ΔCE::WT* complemented strain showed
364 exon exclusion similar to the WT *Mtb* or *Δhsr1::hsr1* infection (Fig. 6E). With the above
365 results, we conclude that hsr1-mediated impact on host RNA splicing was dependent on its
366 secretion in ESX1-dependent manner.
367
368 ***Mtb* hsr1 is a virulence factor and acts by sequestering SNRPF**
369 Results so far show that without hsr1, *Mtb* could not alter the splicing events in the manner
370 caused by the WT strain. We wondered whether this loss of function also impacted the intra-

371 macrophage trajectory of *Mtb*. In *ex vivo* infected THP-1 macrophages, the growth of the
372 *Δhsr1* strain was markedly reduced compared to the WT *Mtb* (Fig. 7A). In agreement with
373 that, *Δhsr1* strain infected macrophages showed increased Cathepsin D staining and also an
374 increase in the co-localization of *Mtb* with Cathepsin D, compared to the WT *Mtb* (Fig. 7B).
375 This suggests that *Δhsr1* strains fail to execute the phagosome maturation arrest as is known
376 for the WT *Mtb* [57]. Since hsr1 was also responsible for binding with SNRPF in the cytoplasm
377 of THP-1 macrophages, we next overexpressed SNRPF in THP-1 macrophages and infected
378 them with WT *Mtb*, expecting that stoichiometric abundance of SNRPF should overcome the
379 impact of hsr1 during WT infection and would help better control of bacterial growth. In
380 THP-1 macrophages expressing SNRPF and infected with WT *Mtb*, we noted increased MFI
381 for SNRPF and a reduction in the bacterial CFU (Fig. 7C). No such effect was seen when
382 another sm Core protein SNRPD2 was overexpressed in these cells (Fig. S6B). We next
383 compared the in vivo infection of Wt and *Δhsr1* strains in the mice model (Fig. 7D). Upon
384 infection in mice, the *Δhsr1* strain was significantly compromised in the establishment of
385 infection compared to the WT *Mtb*, as reflected by a reduced bacterial burden in the lungs of
386 infected mice at 2- and 4- weeks post-infection (Fig. 7E). We also analyzed SNRPF
387 immunostaining in the lung sections of uninfected WT *Mtb*-infected and *Δhsr1*-infected mice
388 with anti-SNRPF antibody. Consistent with the results observed during *ex vivo* infection in
389 THP-1 macrophages, the lung sections from WT *Mtb*-infected mice showed significant
390 accumulation of SNRPF in the extranuclear space, suggesting binding and possible
391 sequestration in the cytoplasm (Fig. 7F). This cytosolic staining of SNRPF was not observed
392 in the lung sections from mice that were infected with *Δhsr1* strain (Fig. 7F). Thus, cytosolic
393 sequestration of SNRPF by *Mtb* protein hsr1 is an important virulence mechanism of *Mtb*.
394
395 **Altered RNA splicing in monocytes from human TB subjects and distinct SNRPF**
396 **dysregulation in the human TB granulomas**
397 To understand the dysregulation of RNA splicing in human TB subjects, we re-analyzed
398 RNAseq data from the monocytes of human pulmonary TB subjects and corresponding
399 healthy contacts[58]. The dataset comprised monocyte transcriptomes from 20 PTB subjects
400 and 19 healthy controls. We analyzed this data set for transcript-level quantification (see
401 methods, table S6). Using all the significantly regulated transcripts, we could observe distinct
402 clustering of PTB subjects and healthy controls in the PCA analysis (Fig. S6C). Among the
403 large number of transcripts showing significant regulation, we focused specifically on

404 transcripts belonging to functional classes like RNA splicing, metabolism, immune response
405 and inflammation. As can be seen from the heat maps in Fig. 8A, based on the level of
406 transcript expression within each of the functional classes, the PTB group could be
407 distinctively identified from the healthy controls. This remarkable observation highlights
408 systemic RNA splicing alterations in tuberculosis patients. Finally, to assess whether an
409 SNRPF-dependent mechanism plays a role in altering RNA splicing in human subjects, we
410 screened human intestinal TB (ITB) granulomas for SNRPF by immunohistochemistry.
411 Consistent with the earlier results from *ex vivo* infection in THP-1 macrophages and *in vivo*
412 infection in mice, the human ITB granulomas showed extensive SNRPF staining (Fig. 8B).
413 Moreover, these staining were more pronounced in the multinucleate giant cells and
414 neighbouring histiocytes (Fig. 8B and S6D). Additionally, we could observe strong cytosolic
415 staining in the granulomas (Fig. 8B). No such distinct staining of SNRPF was noted in the
416 control tissues (Fig. S6E). Similarly, there was no specific staining difference for another sm
417 Core protein SNRPD2 between the control and ITB sections, again underscoring the
418 specificity of the SNRPF-mediated mechanism (Fig. S8). Taken together, using results from
419 *ex vivo* infection, *in vivo* infections and from the human TB subjects, we conclude that
420 SNRPF sequestration and consequent alteration in the host RNA splicing aids bacterial
421 growth and survival within the host, thereby contributing to its pathogenicity.
422

423 **Discussions**

424 The ability of *Mtb* to adapt to the hostile immunological environment in the hosts is
425 remarkable. Almost every physiological process relevant to host immune responses appears
426 to be targeted by the *Mtb,* enabling the pathogen's survival and consequent pathology. This
427 study specifically looked at RNA splicing, a post-transcriptional gene regulation mechanism
428 in the eukaryotes, to understand how *Mtb* achieves the targeted impairment of the seemingly
429 complex process of RNA splicing in the host. As shown earlier by us and others, infection-
430 induced altered RNA splicing helps the bacteria control host responses by preventing the
431 synthesis of target genes in a fully functional form [13,15,59-61]. Considering that RNA splicing is
432 fundamental to eukaryotic gene expression, which in turn is critical for shaping the cellular
433 responses to infection, the mechanistic understanding of this process could have a
434 transformational impact on our ability to develop novel strategies towards controlling TB.
435

436 Since RNA splicing is a multi-step process involving the assembly of a large multi-molecular
437 complex, our working hypothesis was that certain secreted proteins from *Mtb* could interact
438 with and, therefore, interfere in the assembly of spliceosome complexes, thereby altering the
439 pattern of RNA splicing. Proteomic analysis of the spliceosome complexes from the infected
440 macrophages and the Y2H screen between bacterial secretome and host SFs, through
441 independent approaches, did converge to some dysregulation at the level of snRNPs, the key
442 components of spliceosome complexes. The assembly of snRNPs require snRNAs to get
443 transported to the cytoplasm, where they interact with the components of the SMN complex
444 and the heptameric ring called sm Core proteins, together forming the snRNPs, that enter the
445 nucleus and participate in the RNA splicing reactions[23,24,31,50,53]. While the interaction
446 network obtained by Y2H was dense and practically impossible to verify all those
447 interactions through independent techniques, we rationally chose a few *Mtb* genes identified
448 through the Y2H screen for further validation. With the customized assays developed for the
449 purpose, we narrowed down on Rv1435c or hsr1, as the major regulator of host RNA splicing
450 during infection. Apart from our observation of its ability to alter host RNA splicing, there is
451 no defined function of Rv1435c in the literature, making it an attractive target for mechanistic
452 explorations.
453

454 Interestingly, the orthologues of Rv1435c in other mycobacterial species are classified as
455 secreted xylosidase, an activity lacking in the *Mtb* hsr1. Mechanistically, hsr1 allowed *Mtb* to
456 bind in the cytosol with two key components of snRNPs, U5 snRNA and SNRPF.

457 Experiments with SMN complex proteins like GEMIN3 or GEMIN8, smCore proteins like
458 SNRPD2 and snRNAs like U2 snRNA reveal that this interaction was most likely selective
459 with U5 snRNA and SNRPF, and it did not represent the interaction of *Mtb* with whole
460 snRNP complex. Through studies in unrelated systems like neurodegenerative diseases and
461 cancer, it is shown that stoichiometric disbalance of snRNP components like snRNA, SMN
462 complex proteins or smCore proteins can dramatically alter the snRNP complex biogenesis
463 and impact RNA splicing[30,31,34,50,54,62-64]. U5 snRNA is classically known for its role in
464 recognition of the 3' splice site and, therefore, under depleting U5 snRNA condition, there
465 could be a fierce competition between various 3' acceptor splice sites, causing weaker splice
466 junctions to lose out and not get incorporated into the final processed mRNA.
467 Similarly, SNRPF is part of several snRNP complexes, and its dysregulation due to
468 cytoplasmic binding with *Mtb* may have a widespread impact on RNA splicing [31,54,63].
469 Crucially, the nucleo-cytoplasmic shuttling of snRNA for snRNP biogenesis is an
470 evolutionarily conserved quality control mechanism[53]. However, it appears that *Mtb*, through
471 its course of evolution, learnt to disrupt this process without actually going to the nucleus.
472 The snRNP biogenesis defect appears to be operational in the lungs of *Mtb*-infected mice and
473 the human TB granuloma sections. Since human PTB subjects also showed massive
474 alterations in the RNA splicing pattern, to the extent that they could classify healthy from the
475 PTB subjects, it is plausible that this mechanism could cause systemic RNA splicing defect,
476 underlying many pathological states.
477 Interestingly, very limited reports highlight bacterial manipulation of host RNA splicing
478 [13,15,65]. A large number of studies focus on chronic pathology like neurodegenerative
479 disorders or cancer[51,64]. Among infectious diseases, the majority of studies relate to viral
480 infections. However, the mechanism of viral infection-mediated RNA splicing alterations
481 differs from the one reported in this study.
482 Loss of hsr1 in *Mtb* resulted in a compromised growth of bacteria inside human macrophages
483 or in mouse lungs. This observation makes *Mtb* hsr1 a novel virulence factor. While we
484 cannot rule out additional mechanisms, however, since unlike the WT *Mtb*, the *Δhsr1* strains
485 cannot alter host RNA splicing, we propose that losing the ability to alter host RNA splicing
486 compromises the virulence of *Mtb*. This observation makes host RNA splicing regulators and
487 the mycobacterial factors regulating that as a new set of host- and pathogen-directed therapy
488 candidates against TB, respectively.
489

Acknowledgements:

The work was supported by DBT-Wellcome Trust India Alliance Senior Fellowship to DK (IA/S/17/1/503071). The work was also partly supported by grants from SERB (EMR/2016/005296 to DK) and the Department of Biotechnology, Govt of India (BT/IC-06/003/91-Flagship program to DK).

Author Contributions:

Original conceptualization: DK; Experiments: KC, NP, YK, DD, NA, PS, BM, HK, LS, LM; Investigation: KC; Analysis and Visualization: KC, MD, DK; Resources: VN, AS, VA, PD; Supervision: DK; Writing-original draft: DK, KC, MD, NP; Writing—review & editing: VN, AS, PD, DK

Conflict of Interest:

The authors declare no conflict of interest.

505 **References:**

506

507 1 Augenstreich, J. & Briken, V. Host Cell Targets of Released Lipid and Secreted Protein
508 Effectors of Mycobacterium tuberculosis. *Front Cell Infect Microbiol* **10**, 595029
509 (2020). https://doi.org/10.3389/fcimb.2020.595029
510 2 Chandra, P. *et al.* Mycobacterium tuberculosis Inhibits RAB7 Recruitment to
511 Selectively Modulate Autophagy Flux in Macrophages. *Sci Rep* **5**, 16320 (2015).
512 https://doi.org/10.1038/srep16320
513 3 de Martino, M., Lodi, L., Galli, L. & Chiappini, E. Immune Response to Mycobacterium
514 tuberculosis: A Narrative Review. *Front Pediatr* **7**, 350 (2019).
515 https://doi.org/10.3389/fped.2019.00350
516 4 Ernst, J. D. The immunological life cycle of tuberculosis. *Nat Rev Immunol* **12**, 581-
517 591 (2012). https://doi.org/10.1038/nri3259
518 5 Flynn, J. L. & Chan, J. Immunology of tuberculosis. *Annu Rev Immunol* **19**, 93-129
519 (2001). https://doi.org/10.1146/annurev.immunol.19.1.93
520 6 Kumar, D. & Rao, K. V. Regulation between survival, persistence, and elimination of
521 intracellular mycobacteria: a nested equilibrium of delicate balances. *Microbes Infect*
522 **13**, 121-133 (2011). https://doi.org/10.1016/j.micinf.2010.10.009
523 7 Zhai, W., Wu, F., Zhang, Y., Fu, Y. & Liu, Z. The Immune Escape Mechanisms of
524 Mycobacterium Tuberculosis. *Int J Mol Sci* **20** (2019).
525 https://doi.org/10.3390/ijms20020340
526 8 Karim, A. F. *et al.* Express path analysis identifies a tyrosine kinase Src-centric
527 network regulating divergent host responses to Mycobacterium tuberculosis
528 infection. *J Biol Chem* **286**, 40307-40319 (2011).
529 https://doi.org/10.1074/jbc.M111.266239
530 9 Koul, A., Herget, T., Klebl, B. & Ullrich, A. Interplay between mycobacteria and host
531 signalling pathways. *Nat Rev Microbiol* **2**, 189-202 (2004).
532 https://doi.org/10.1038/nrmicro840
533 10 Lavalett, L. *et al.* Alveolar macrophages from tuberculosis patients display an altered
534 inflammatory gene expression profile. *Tuberculosis (Edinb)* **107**, 156-167 (2017).
535 https://doi.org/10.1016/j.tube.2017.08.012
536 11 Lesho, E. *et al.* Transcriptional responses of host peripheral blood cells to
537 tuberculosis infection. *Tuberculosis (Edinb)* **91**, 390-399 (2011).
538 https://doi.org/10.1016/j.tube.2011.07.002
539 12 McGarvey, J. A., Wagner, D. & Bermudez, L. E. Differential gene expression in
540 mononuclear phagocytes infected with pathogenic and non-pathogenic
541 mycobacteria. *Clin Exp Immunol* **136**, 490-500 (2004).
542 https://doi.org/10.1111/j.1365-2249.2004.02490.x
543 13 Kalam, H., Fontana, M. F. & Kumar, D. Alternate splicing of transcripts shape
544 macrophage response to Mycobacterium tuberculosis infection. *PLoS Pathog* **13**,
545 e1006236 (2017). https://doi.org/10.1371/journal.ppat.1006236
546 14 Kalam, H., Singh, K., Chauhan, K., Fontana, M. F. & Kumar, D. Alternate splicing of
547 transcripts upon Mycobacterium tuberculosis infection impacts the expression of
548 functional protein domains. *IUBMB Life* **70**, 845-854 (2018).
549 https://doi.org/10.1002/iub.1887

15 Chauhan, K., Kalam, H., Dutt, R. & Kumar, D. RNA Splicing: A New Paradigm in Host-Pathogen Interactions. *J Mol Biol* **431**, 1565-1575 (2019). https://doi.org/10.1016/j.jmb.2019.03.001

16 Artemyeva-Isman, O. V. & Porter, A. C. G. U5 snRNA Interactions With Exons Ensure Splicing Precision. *Front Genet* **12**, 676971 (2021). https://doi.org/10.3389/fgene.2021.676971

17 Lee, Y. & Rio, D. C. Mechanisms and Regulation of Alternative Pre-mRNA Splicing. *Annu Rev Biochem* **84**, 291-323 (2015). https://doi.org/10.1146/annurev-biochem-060614-034316

18 Matera, A. G. & Wang, Z. A day in the life of the spliceosome. *Nat Rev Mol Cell Biol* **15**, 108-121 (2014). https://doi.org/10.1038/nrm3742

19 Papasaikas, P., Tejedor, J. R., Vigevani, L. & Valcarcel, J. Functional splicing network reveals extensive regulatory potential of the core spliceosomal machinery. *Mol Cell* **57**, 7-22 (2015). https://doi.org/10.1016/j.molcel.2014.10.030

20 Schlautmann, L. P. & Gehring, N. H. A Day in the Life of the Exon Junction Complex. *Biomolecules* **10** (2020). https://doi.org/10.3390/biom10060866

21 Wahl, M. C., Will, C. L. & Luhrmann, R. The spliceosome: design principles of a dynamic RNP machine. *Cell* **136**, 701-718 (2009). https://doi.org/10.1016/j.cell.2009.02.009

22 Wilkinson, M. E., Charenton, C. & Nagai, K. RNA Splicing by the Spliceosome. *Annu Rev Biochem* **89**, 359-388 (2020). https://doi.org/10.1146/annurev-biochem-091719-064225

23 Gubitz, A. K., Feng, W. & Dreyfuss, G. The SMN complex. *Exp Cell Res* **296**, 51-56 (2004). https://doi.org/10.1016/j.yexcr.2004.03.022

24 Karijolich, J. & Yu, Y. T. Spliceosomal snRNA modifications and their function. *RNA Biol* **7**, 192-204 (2010). https://doi.org/10.4161/rna.7.2.11207

25 Liu, J. L. & Gall, J. G. U bodies are cytoplasmic structures that contain uridine-rich small nuclear ribonucleoproteins and associate with P bodies. *Proc Natl Acad Sci U S A* **104**, 11655-11659 (2007). https://doi.org/10.1073/pnas.0704977104

26 Patel, S. B. & Bellini, M. The assembly of a spliceosomal small nuclear ribonucleoprotein particle. *Nucleic Acids Res* **36**, 6482-6493 (2008). https://doi.org/10.1093/nar/gkn658

27 Pellizzoni, L. Chaperoning ribonucleoprotein biogenesis in health and disease. *EMBO Rep* **8**, 340-345 (2007). https://doi.org/10.1038/sj.embor.7400941

28 Shaw, D. J., Eggleton, P. & Young, P. J. Joining the dots: production, processing and targeting of U snRNP to nuclear bodies. *Biochim Biophys Acta* **1783**, 2137-2144 (2008). https://doi.org/10.1016/j.bbamcr.2008.07.025

29 Yong, J., Kasim, M., Bachorik, J. L., Wan, L. & Dreyfuss, G. Gemin5 delivers snRNA precursors to the SMN complex for snRNP biogenesis. *Mol Cell* **38**, 551-562 (2010). https://doi.org/10.1016/j.molcel.2010.03.014

30 Zhang, R. *et al.* Structure of a key intermediate of the SMN complex reveals Gemin2's crucial function in snRNP assembly. *Cell* **146**, 384-395 (2011). https://doi.org/10.1016/j.cell.2011.06.043

31 Zhang, Z. *et al.* SMN deficiency causes tissue-specific perturbations in the repertoire of snRNAs and widespread defects in splicing. *Cell* **133**, 585-600 (2008). https://doi.org/10.1016/j.cell.2008.03.031

596 32 Strasser, A., Dickmanns, A., Luhrmann, R. & Ficner, R. Structural basis for m3G-cap-
597 mediated nuclear import of spliceosomal UsnRNPs by snurportin1. *EMBO J* **24**, 2235-
598 2243 (2005). https://doi.org/10.1038/sj.emboj.7600701
599 33 Wang, Z. & Burge, C. B. Splicing regulation: from a parts list of regulatory elements to
600 an integrated splicing code. *RNA* **14**, 802-813 (2008).
601 https://doi.org/10.1261/rna.876308
602 34 Cartegni, L., Hastings, M. L., Calarco, J. A., de Stanchina, E. & Krainer, A. R.
603 Determinants of exon 7 splicing in the spinal muscular atrophy genes, SMN1 and
604 SMN2. *Am J Hum Genet* **78**, 63-77 (2006). https://doi.org/10.1086/498853
605 35 Pai, A. A. *et al.* Widespread Shortening of 3' Untranslated Regions and Increased
606 Exon Inclusion Are Evolutionarily Conserved Features of Innate Immune Responses
607 to Infection. *PLoS Genet* **12**, e1006338 (2016).
608 https://doi.org/10.1371/journal.pgen.1006338
609 36 Penn, B. H. *et al.* An Mtb-Human Protein-Protein Interaction Map Identifies a Switch
610 between Host Antiviral and Antibacterial Responses. *Mol Cell* **71**, 637-648 e635
611 (2018). https://doi.org/10.1016/j.molcel.2018.07.010
612 37 Portal-Celhay, C. *et al.* Mycobacterium tuberculosis EsxH inhibits ESCRT-dependent
613 CD4(+) T-cell activation. *Nat Microbiol* **2**, 16232 (2016).
614 https://doi.org/10.1038/nmicrobiol.2016.232
615 38 Sharma, G., Upadhyay, S., Srilalitha, M., Nandicoori, V. K. & Khosla, S. The interaction
616 of mycobacterial protein Rv2966c with host chromatin is mediated through non-CpG
617 methylation and histone H3/H4 binding. *Nucleic Acids Res* **43**, 3922-3937 (2015).
618 https://doi.org/10.1093/nar/gkv261
619 39 Yaseen, I., Kaur, P., Nandicoori, V. K. & Khosla, S. Mycobacteria modulate host
620 epigenetic machinery by Rv1988 methylation of a non-tail arginine of histone H3.
621 *Nat Commun* **6**, 8922 (2015). https://doi.org/10.1038/ncomms9922
622 40 Klimesova, K. *et al.* TSSC4 is a component of U5 snRNP that promotes tri-snRNP
623 formation. *Nat Commun* **12**, 3646 (2021). https://doi.org/10.1038/s41467-021-
624 23934-y
625 41 Neuenkirchen, N. *et al.* Reconstitution of the human U snRNP assembly machinery
626 reveals stepwise Sm protein organization. *EMBO J* **34**, 1925-1941 (2015).
627 https://doi.org/10.15252/embj.201490350
628 42 Malakar, B. *et al.* Phosphorylation of CFP10 modulates Mycobacterium tuberculosis
629 virulence. *mBio* **14**, e0123223 (2023). https://doi.org/10.1128/mbio.01232-23
630 43 de Souza, G. A., Leversen, N. A., Malen, H. & Wiker, H. G. Bacterial proteins with
631 cleaved or uncleaved signal peptides of the general secretory pathway. *J Proteomics*
632 **75**, 502-510 (2011). https://doi.org/10.1016/j.jprot.2011.08.016
633 44 Malen, H., Berven, F. S., Fladmark, K. E. & Wiker, H. G. Comprehensive analysis of
634 exported proteins from Mycobacterium tuberculosis H37Rv. *Proteomics* **7**, 1702-
635 1718 (2007). https://doi.org/10.1002/pmic.200600853
636 45 Mehra, A. *et al.* Mycobacterium tuberculosis type VII secreted effector EsxH targets
637 host ESCRT to impair trafficking. *PLoS Pathog* **9**, e1003734 (2013).
638 https://doi.org/10.1371/journal.ppat.1003734
639 46 Bonano, V. I., Oltean, S. & Garcia-Blanco, M. A. A protocol for imaging alternative
640 splicing regulation in vivo using fluorescence reporters in transgenic mice. *Nat Protoc*
641 **2**, 2166-2181 (2007). https://doi.org/10.1038/nprot.2007.292

47 Luan, X. *et al.* High Immunogenicity of a T-Cell Epitope-Rich Recombinant Protein Rv1566c-444 From Mycobacterium tuberculosis in Immunized BALB/c Mice, Despite Its Low Diagnostic Sensitivity. *Front Immunol* **13**, 824415 (2022). https://doi.org/10.3389/fimmu.2022.824415

48 Varadi, M. *et al.* AlphaFold Protein Structure Database in 2024: providing structure coverage for over 214 million protein sequences. *Nucleic Acids Res* **52**, D368-D375 (2024). https://doi.org/10.1093/nar/gkad1011

49 van Kessel, J. C. & Hatfull, G. F. Recombineering in Mycobacterium tuberculosis. *Nat Methods* **4**, 147-152 (2007). https://doi.org/10.1038/nmeth996

50 Massenet, S., Pellizzoni, L., Paushkin, S., Mattaj, I. W. & Dreyfuss, G. The SMN complex is associated with snRNPs throughout their cytoplasmic assembly pathway. *Mol Cell Biol* **22**, 6533-6541 (2002). https://doi.org/10.1128/MCB.22.18.6533-6541.2002

51 Wood, K. A., Eadsforth, M. A., Newman, W. G. & O'Keefe, R. T. The Role of the U5 snRNP in Genetic Disorders and Cancer. *Front Genet* **12**, 636620 (2021). https://doi.org/10.3389/fgene.2021.636620

52 Will, C. L. *et al.* A novel U2 and U11/U12 snRNP protein that associates with the pre-mRNA branch site. *EMBO J* **20**, 4536-4546 (2001). https://doi.org/10.1093/emboj/20.16.4536

53 Becker, D. *et al.* Nuclear Pre-snRNA Export Is an Essential Quality Assurance Mechanism for Functional Spliceosomes. *Cell Rep* **27**, 3199-3214 e3193 (2019). https://doi.org/10.1016/j.celrep.2019.05.031

54 Jia, Y., Mu, J. C. & Ackerman, S. L. Mutation of a U2 snRNA gene causes global disruption of alternative splicing and neurodegeneration. *Cell* **148**, 296-308 (2012). https://doi.org/10.1016/j.cell.2011.11.057

55 Groschel, M. I., Sayes, F., Simeone, R., Majlessi, L. & Brosch, R. ESX secretion systems: mycobacterial evolution to counter host immunity. *Nat Rev Microbiol* **14**, 677-691 (2016). https://doi.org/10.1038/nrmicro.2016.131

56 Stoop, E. J., Bitter, W. & van der Sar, A. M. Tubercle bacilli rely on a type VII army for pathogenicity. *Trends Microbiol* **20**, 477-484 (2012). https://doi.org/10.1016/j.tim.2012.07.001

57 Vergne, I. *et al.* Mycobacterium tuberculosis phagosome maturation arrest: mycobacterial phosphatidylinositol analog phosphatidylinositol mannoside stimulates early endosomal fusion. *Mol Biol Cell* **15**, 751-760 (2004). https://doi.org/10.1091/mbc.e03-05-0307

58 Del Rosario, R. C. H. *et al.* Histone acetylome-wide associations in immune cells from individuals with active Mycobacterium tuberculosis infection. *Nat Microbiol* **7**, 312-326 (2022). https://doi.org/10.1038/s41564-021-01049-w

59 Denisenko, E. *et al.* Transcriptionally induced enhancers in the macrophage immune response to Mycobacterium tuberculosis infection. *BMC Genomics* **20**, 71 (2019). https://doi.org/10.1186/s12864-019-5450-6

60 Louadi, Z. *et al.* DIGGER: exploring the functional role of alternative splicing in protein interactions. *Nucleic Acids Res* **49**, D309-D318 (2021). https://doi.org/10.1093/nar/gkaa768

61 Bradley, R. K. & Anczukow, O. RNA splicing dysregulation and the hallmarks of cancer. *Nat Rev Cancer* (2023). https://doi.org/10.1038/s41568-022-00541-7

688 62 Boudreault, S. *et al.* Reovirus mu2 protein modulates host cell alternative splicing by
689 reducing protein levels of U5 snRNP core components. *Nucleic Acids Res* **50**, 5263-
690 5281 (2022). https://doi.org/10.1093/nar/gkac272
691 63 De Maio, F. A. *et al.* The Dengue Virus NS5 Protein Intrudes in the Cellular
692 Spliceosome and Modulates Splicing. *PLoS Pathog* **12**, e1005841 (2016).
693 https://doi.org/10.1371/journal.ppat.1005841
694 64 Almstead, L. L. & Sarnow, P. Inhibition of U snRNP assembly by a virus-encoded
695 proteinase. *Genes Dev* **21**, 1086-1097 (2007). https://doi.org/10.1101/gad.1535607
696 65 Corre, M. *et al.* Alternative splicing induced by bacterial pore-forming toxins
697 sharpens CIRBP-mediated cell response to Listeria infection. *Nucleic Acids Res* **51**,
698 12459-12475 (2023). https://doi.org/10.1093/nar/gkad1033
699

700

701 **Figure Legends:**
702
703 **Figure 1: Dysregulation of host RNA splicing machinery in Mtb-infected macrophages**
704 **A)** The schematic representation of perturbed alternative splicing resulting in exon
705 skipping events upon *Mtb* infection.
706 **B)** A schematic model depicting the ordered pathway of mRNA transcription by RNAP II
707 and splicing catalysed by spliceosome complex. The U1snRNP binds the 5' splice site
708 and U2 snRNP binds the branch point adenine to form complex A. U4/U5.U6 snRNP
709 binds to form complex B and causes conformational changes to form activated complex
710 B. This is followed by the first transesterification reaction, releasing U1 and U4 snRNP
711 and the second transesterification reaction forming complex C, releasing the lariat
712 intron and U2, U5 and U6 snRNP. The U snRNP are the major players in splicing
713 catalysis.
714 **C)** The schematic of the spliceosome complex pulldown from the *Mtb* infected THP-1
715 macrophages 48 hours post-infection for Mass Spectrometry.
716 **D)** Heatmap shows massive dysregulation in the level and cellular distribution of human
717 proteins involved in RNA splicing and identified in MS of the spliceosome complex
718 pulldown from the *Mtb* infected THP-1 macrophages 48 hours post-infection. The three
719 boxes depict proteins that show depletion (green), depletion and mislocalisation (blue)
720 and mislocalisation (red) patterns in Mtb-infected cells compared to the uninfected
721 cells.
722
723 **Figure 2: Mycobacterial secretory proteins and host spliceosome proteins interactome.**
724 A) The schematic flow chart for high throughput one-to-one Y2H assay in 1536 well
725 format. Protein pairs showing interaction in 3 or 4 biological replicates were considered
726 as positive interactions.
727 B) *Mtb* proteins -host splicing factor interactome- the positive interactions from the Y2H
728 screen were used to generate the network shown here. The diamond and circle represent
729 the host and *Mtb* proteins, respectively, and the size corresponds to the number of
730 interactions observed. The proteins coloured yellow in the network are described
731 further in the subsequent sections.
732 C) The Venn diagrams show proteins belonging to the major spliceosome components and
733 their corresponding overlap with the interacting *Mtb* proteins.
734
735 **Figure 3: *Ex vivo* infection assays and reporter assays to test the role of *Mtb* proteins in**
736 **host RNA splicing**
737
738 A) Designing of the custom *in vivo* fluorescent splicing reporter. Schematic for the
739 constitutive splicing reporter pRint with a short adenovirus intron intervening the
740 DsRed gene with a strong 5' and 3' splice sites. In the pGint splicing constructs, the
741 alternative exon of ACADVL, DDX11, DDX42, ACSL1 and NFYA, along with the
742 flanking 100bp intronic sequences, were inserted within eGFP reading frame. The exon
743 disrupts the reading frame, however, skipping of the test exon reconstitutes EGFP
744 fluorescence.

745 B) In cell reporter assay: the pRint expressing stable HEK293T cell lines were co-
746 transfected with a pGint construct and pDest-FLAG construct encoding proteins
747 Rv1252c (NIC), Rv1566c, Rv1435c, Rv1643, or empty vector control, followed by
748 Flow cytometry. In the $DsRed^+$ gate, the $\%FITC^+$ population was calculated to measure
749 the extent of the test exon-skipping event.
750 C) $\%FITC^+$ population for each of the indicated reporter constructs in the presence of
751 indicated mycobacterial protein, non-interacting control, or vector controls. Each dot
752 represents an independent biological replicate (N=3), indicating p values from One-
753 way ANOVA.
754 D) Validation of physical interactions between indicated pairs of Rv1435c proteins
755 (FLAG-tagged) and host proteins – (HA-tagged) in HEK293T cells. Data is
756 representative of two or more biologically independent transfection and pulldown
757 experiments.
758 E) The schematic representation of infecting THP-1 macrophages with *Msmeg* strains that
759 express Rv1435c under IVN inducible promotor followed by RTPCT for assessing
760 target gene splicing event.
761 F) Isoform-specific qPCR to assess the impact of Rv1435c expressing *Msmeg* infection in
762 THP-1 macrophages on exon skipping event in DDX11, N=3, indicating p values from
763 One-way ANOVA.
764
765 **Figure 4: Role of Mtb Rv1435c protein in altering host RNA splicing.**
766
767 A) The schematic of knocking out the *Rv1435c* or *hsr1* gene in H37Rv using the
768 recombineering approach. Positive colonies were screened with the primers F1-F3
769 (forward) & R1-R3 (reverse), as shown by the arrows.
770 B) Agarose gel electrophoresis to confirm the replacement of 609bp product (*Rv1435c*)
771 with 1.4Kb hygromycin cassette in the knockout line (F1-R1), absence of hyg in the
772 WT (F2-R2 and F3-R3) and control segment (*rbpA*).
773 C) Q-PCR to show the loss of expression of *Rv1435c* in the knockout strain
774 D) Q-PCR for the target transcripts as mentioned after infection with H37Rv, H37Rv*Δhsr1*
775 and H37Rv*Δhsr1::WT* strain. Data from three biological replicates (N=3), indicating p-
776 values from a one-way ANOVA analysis.
777
778 **Figure 5: Direct interaction of U5 snRNA with Mtb phagosomes.**
779 A) Schematic representation of U snRNA nucleo-cytoplasmic trajectory and assembly of
780 Sm core ring on snRNA by SMN complex to form snRNPs
781 B) Representative images for RNA FISH against U5 snRNA in THP-1 macrophages upon
782 *Mtb* (mCherry-H37Rv) infection at 24- and 48-hrs post-infection. The U5 snRNA probe
783 was labelled with Alexa 488 (green), and the nucleus was stained with DAPI (blue).
784 C) Plots show quantification of U5 snRNA FISH MFI in uninfected and *Mtb*-infected
785 macrophages at 24 ad 48 hpi.
786 D) Direct interaction between H37Rv (red) and U5snRNA at 24- and 48-hrs post-infection.
787 U5snRNA puncta within 0.2 microns from the H37Rv surface are shown as green dots
788 on the 3-D constructed Mtb contours. The 3D reconstruction of the nucleus, U5 snRNA

789 foci and bacteria (see methods) was done to show the U5 snRNA Foci at <0.2 microns
790 distance from the bacterial phagosomes. The quantification of interacting U5 snRNA
791 punctas is shown in the plot at the right. Scale bar: 2 µm.
792 E) Representative image for the U5snRNA FISH in THP-1 macrophages infected with
793 mCherry expressing WT H37Rv or H37Rv*Δhsr1* strains. The plots at the right show
794 the ratio of interacting to non-interacting U5snRNA with WT H37Rv or H37Rv*Δhsr1*.
795 Data is from three biological experiments, two fields each, representing p-value from a
796 Student's t-test analysis.
797
798 **Figure 6: *Mtb* hsr1 secretion is ESX1-dependent, and impacts host RNA splicing by**
799 **sequestering SNRPF**
800 A) Image showing SNRPF colocalising with bacterial phagosomes. The 3D reconstruction
801 of the nucleus, SNRPF foci and bacteria (see methods) was done to show the SNRPF
802 Foci at <0.2 microns distance from the bacterial phagosomes. Scale bar: 2 µm and p
803 values indicate Student's t-test.
804 B) Representative images of SNRPF staining in THP-1 macrophages infected with WT
805 H37Rv or H37Rv*Δhsr1* strains. For the plot below, the number of SNRPF puncta within
806 0.2 microns from the H37Rv surface was counted as interacting and shown as the ratio
807 of interacting to non-interacting SNRPF with WT H37Rv or H37Rv*Δhsr1*. Data is from
808 three biological replicates with two or more fields per slide, representing p-values from
809 Student's t-test.
810 C) Validation of physical interactions between Rv1435c (FLAG-tagged) and SNRPF (HA-
811 tagged) in HEK293T cells using co-immunoprecipitation. Data is representative of two
812 or more biologically independent transfection and pulldown experiments.
813 *D)* Representative images of THP1-macrophages stained with DAPI (nucleus) and
814 Rv1435c antisera (green) upon infection with mCherry expressing WT H37Rv, *Δhsr1,*
815 *Δhsr1::WT, ΔCE* and *ΔCE::WT* strains. Images are representative of two independent
816 biological experiments. Scale bar-2 µm.
817 *E)* The exon-skipping event in ACADVL and ACSL1 transcripts upon infection with WT
818 H37Rv, H37Rv*ΔCE* and H37Rv*ΔCE::WT* at 48hpi from three biologically independent
819 experiments. The p values are from One-way ANOVA.
820
821 **Figure 7: Regulation of host alternative splicing as a virulence mechanism**
822 A) THP-1 macrophages were infected with WT H37Rv or *Δhsr1* strains. At 48 hours post-
823 infection, bacterial load was examined using CFU plating. Data represent fold change
824 in CFU at 48 hrs compared to 0 hr post-infection. (N=3), p values are from Student's t-
825 test.
826 B) The plot shows quantification for staining of cathepsin D in THP1 macrophages
827 infected with WT H37Rv and *Δhsr1*at 48hpi. The different parameters plotted show
828 overall MFI (MFI/cell) and the ratio of cathepsin D foci interacting with bacterial
829 phagosomes (int/non-int). Each dot represents a field analyzed, and an average of a
830 hundred cells are quantified, representing p-values from one-way ANOVA (MFI) or
831 Student's t-test (Int/non-Int).

C) The plot shows quantification (MFI/cell) for staining of SNRPF in WT THP1 macrophages and THP1*::SNRPF* infected with WT H37Rv at 48hpi. Each dot represents a field analyzed, and an average of a hundred cells are quantified. The plot on the right shows the bacterial survival after 48 hours post-infection in WT THP1 and THP1*::SNRPF*. Each dot represents an independent biological experiment. Indicated p values represent Student's t-test.

D) Schematic for study design using mice model of infection

E) BALB/C mice (6-8 weeks old) were infected with 200 CFU of WT H37Rv and *Δhsr1* in separate experiments. At 2- and 4- weeks post-infection, bacterial load in the lungs of the animals was determined by CFU plating. N=6, representing p-values from Student's t-test.

F) The 4-week post-infection lung tissue sections of uninfected, WT H37Rv and Δhsr1 were stained with DAPI (nucleus) and anti-SNRPF antibody. Scale bar: 20 µm

Figure 8: Altered RNA splicing and distinct SNRPF dysregulation in the granulomas of human TB subjects.

A) RNAseq data from the monocytes of pulmonary TB cases (N=20) and healthy contacts (N=19) was analyzed to assess the expression of differential alternatively spliced transcripts. Genes belonging to the indicated functional classes were selected for the cluster analysis. Cluster 1 in each case shows transcripts upregulated in PTB cases.

B) Biopsy sections from human intestinal tuberculosis granulomatous lesions were stained with anti-SNRPF antibody. The arrows indicate multinucleated giant cells with intense staining for cytosolic SNRPF. Black arrows show areas of intense SNRPF staining in the granulomas and in the giant cells.

Figure 9: A model to show *Mtb*-mediated alteration of host RNA splicing by blocking the snRNP biogenesis and post-transcriptional gene regulation in the macrophages.

Figure 1

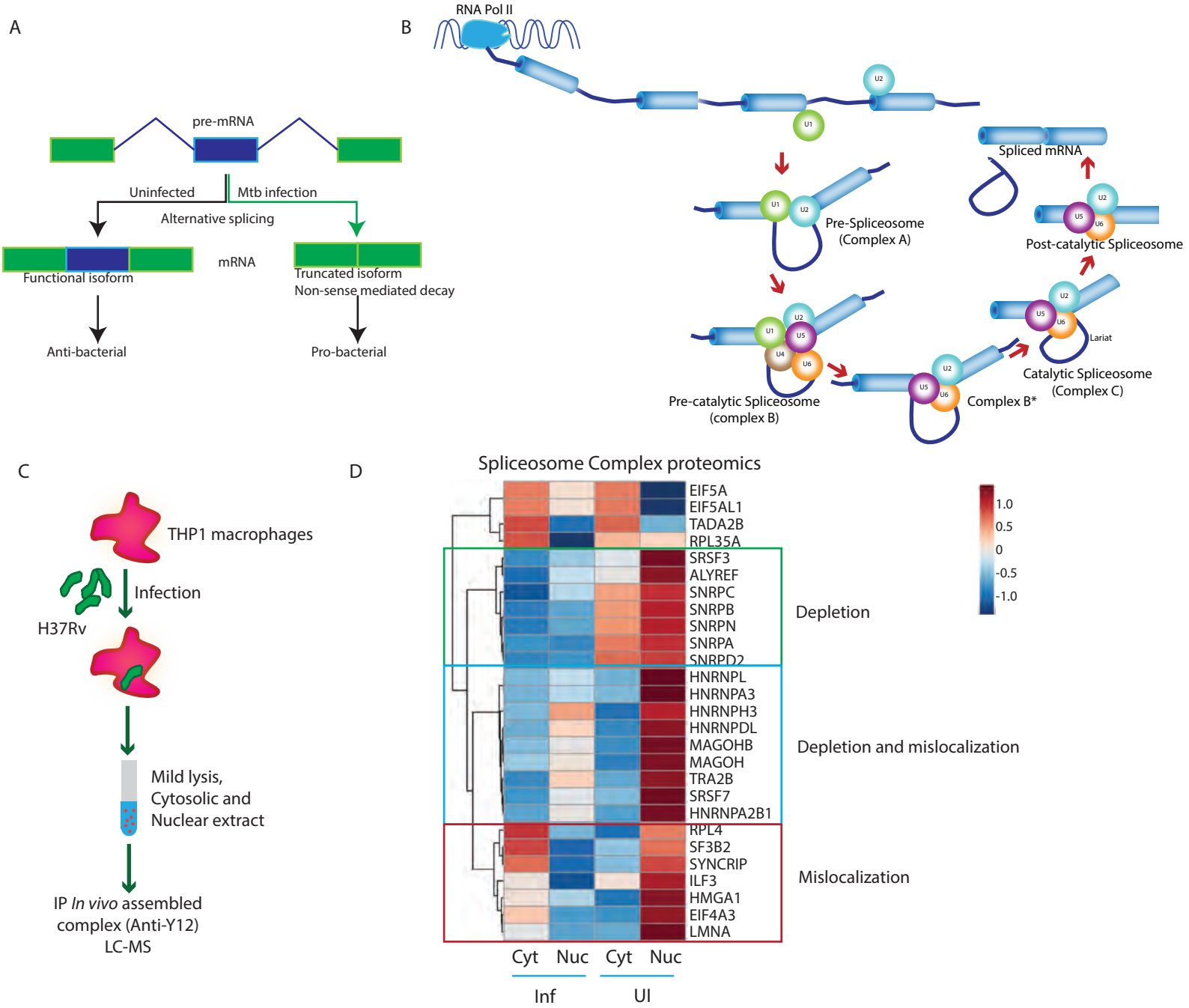
A
pre-mRNA
Uninfected
Mtb infection
Alternative splicing
mRNA
Functional isoform
Truncated isoform
Non-sense mediated decay
Anti-bacterial
Pro-bacterial
B
RNA Pol II
U1
U2
Pre-Spliceosome
(Complex A)
Spliced mRNA
Post-catalytic Spliceosome
U4
U5
U6
Lariat
Pre-catalytic Spliceosome
(complex B)
Complex B*
Catalytic Spliceosome
(Complex C)
C
THP1 macrophages
Infection
H37Rv
Mild lysis,
Cytosolic and
Nuclear extract
IP *In vivo* assembled
complex (Anti-Y12)
LC-MS
D
Spliceosome Complex proteomics
EIF5A
EIF5AL1
TADA2B
RPL35A
SRSF3
ALYREF
SNRPC
SNRPB
SNRPN
SNRPA
SNRPD2
HNRNPL
HNRNPA3
HNRNPH3
HNRNPDL
MAGOHB
MAGOH
TRA2B
SRSF7
HNRNPA2B1
RPL4
SF3B2
SYNCRIP
ILF3
HMGA1
EIF4A3
LMNA
Depletion
Depletion and mislocalization
Mislocalization
1.0
0.5
0
-0.5
-1.0
Cyt
Nuc
Cyt
Nuc
Inf
UI

Figure 2

A

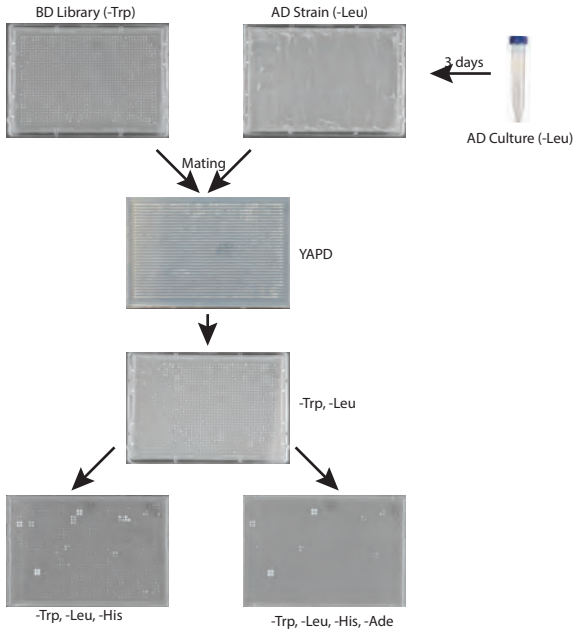
BD Library (-Trp)
AD Strain (-Leu)
3 days
AD Culture (-Leu)
Mating
YAPD
-Trp, -Leu
-Trp, -Leu, -His
-Trp, -Leu, -His, -Ade

B

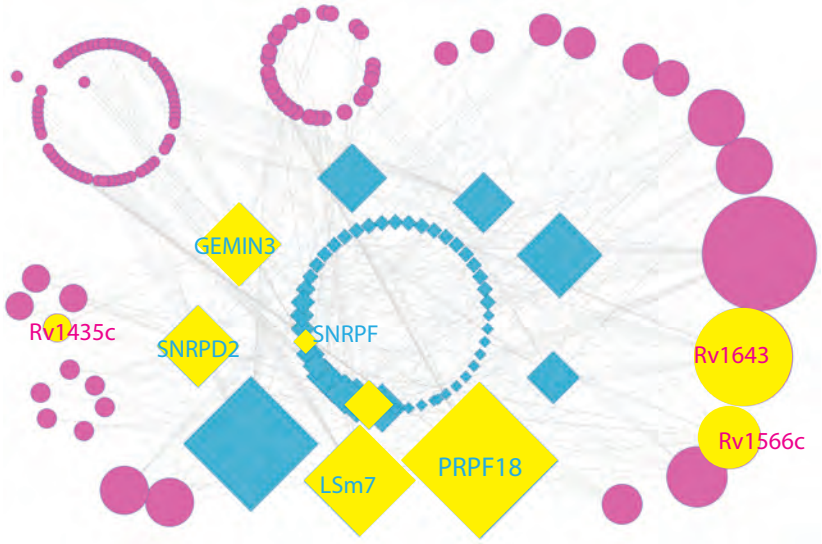
GEMIN3
Rv1435c
SNRPD2
SNRPF
Rv1643
Rv1566c
LSm7
PRPF18

C

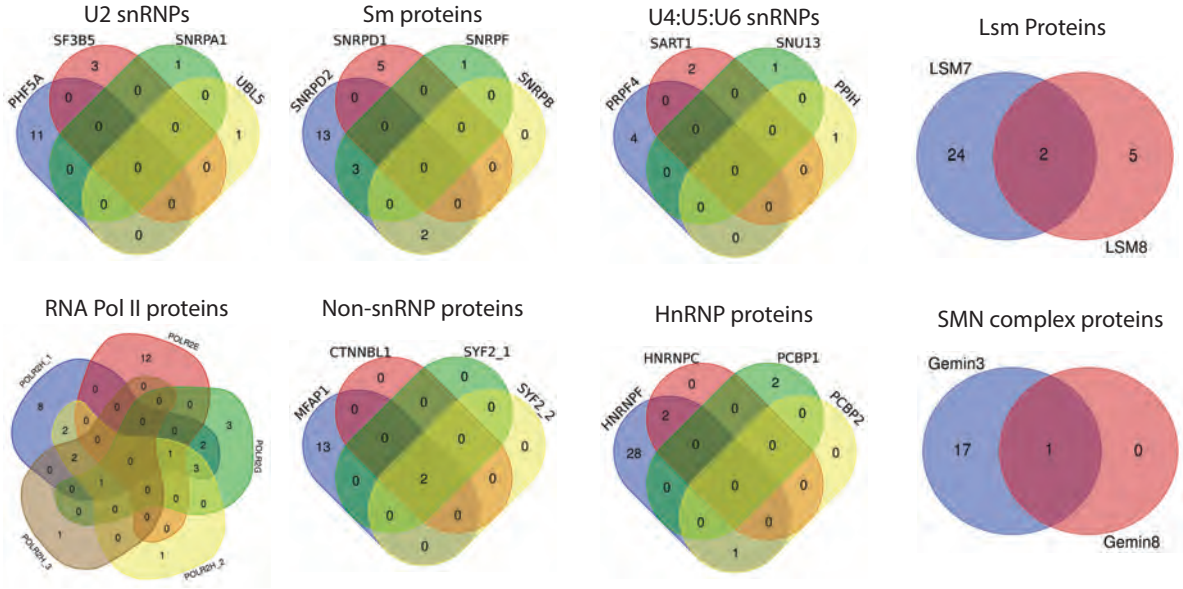
U2 snRNPs
SF3B5
SNRPA1
PHF5A
UBL5
Sm proteins
SNRPD1
SNRPF
SNRPD2
SNRPB
U4:U5:U6 snRNPs
SART1
SNU13
PRPF4
PPIH
Lsm Proteins
LSM7
24
2
5
LSM8
RNA Pol II proteins
POLR2E
POLR2H
Non-snRNP proteins
CTNNBL1
SYF2_1
MFAP1
SYF2_2
HnRNP proteins
HNRNPC
PCBP1
HNRNPF
PCBP2
SMN complex proteins
Gemin3
17
1
0
Gemin8

Figure 3

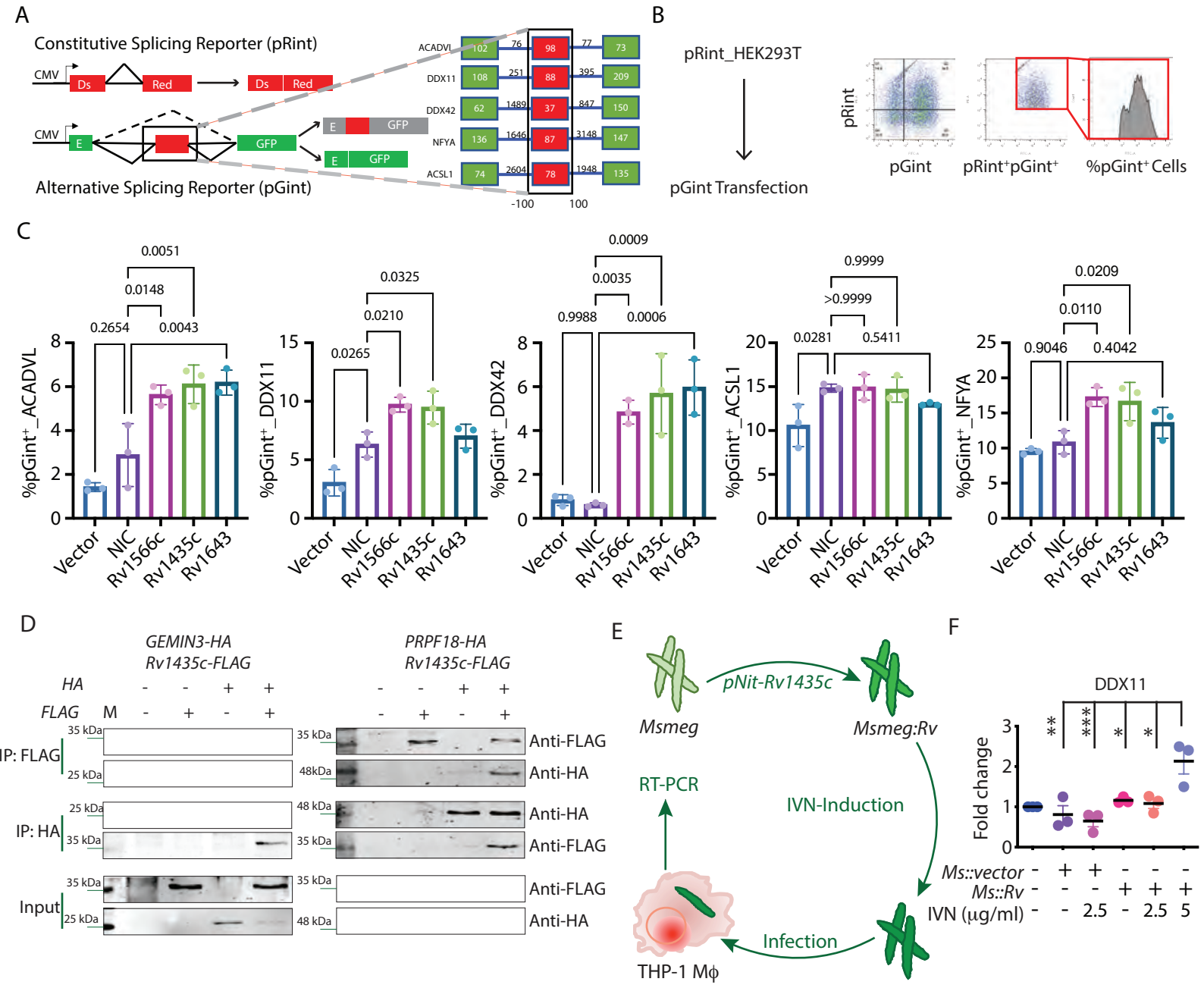
A
Constitutive Splicing Reporter (pRint)
CMV
Ds
Red
Ds
Red
CMV
E
GFP
E
GFP
E
GFP
Alternative Splicing Reporter (pGint)
ACADVL
DDX11
DDX42
NFYA
ACSL1
102
76
98
77
73
108
251
88
395
209
62
1489
37
847
150
136
1646
87
3148
147
74
2604
78
1948
135
-100
100
B
pRint_HEK293T
pGint Transfection
pRint
pGint
pRint+pGint+
%pGint+ Cells
C
%pGint+_ACADVL
%pGint+_DDX11
%pGint+_DDX42
%pGint+_ACSL1
%pGint+_NFYA
0.0051
0.0148
0.2654
0.0043
0.0325
0.0210
0.0265
0.0009
0.0035
0.9988
0.0006
0.9999
>0.9999
0.0281
0.5411
0.0209
0.0110
0.9046
0.4042
Vector
NIC
Rv1566c
Rv1435c
Rv1643
D
GEMIN3-HA
Rv1435c-FLAG
PRPF18-HA
Rv1435c-FLAG
HA
FLAG
M
IP: FLAG
IP: HA
Input
35 kDa
25 kDa
48 kDa
Anti-FLAG
Anti-HA
E
Msmeg
pNit-Rv1435c
Msmeg:Rv
IVN-Induction
Infection
THP-1 Mϕ
RT-PCR
F
DDX11
Fold change
Ms::vector
Ms::Rv
IVN (µg/ml)
2.5
5

Figure 4

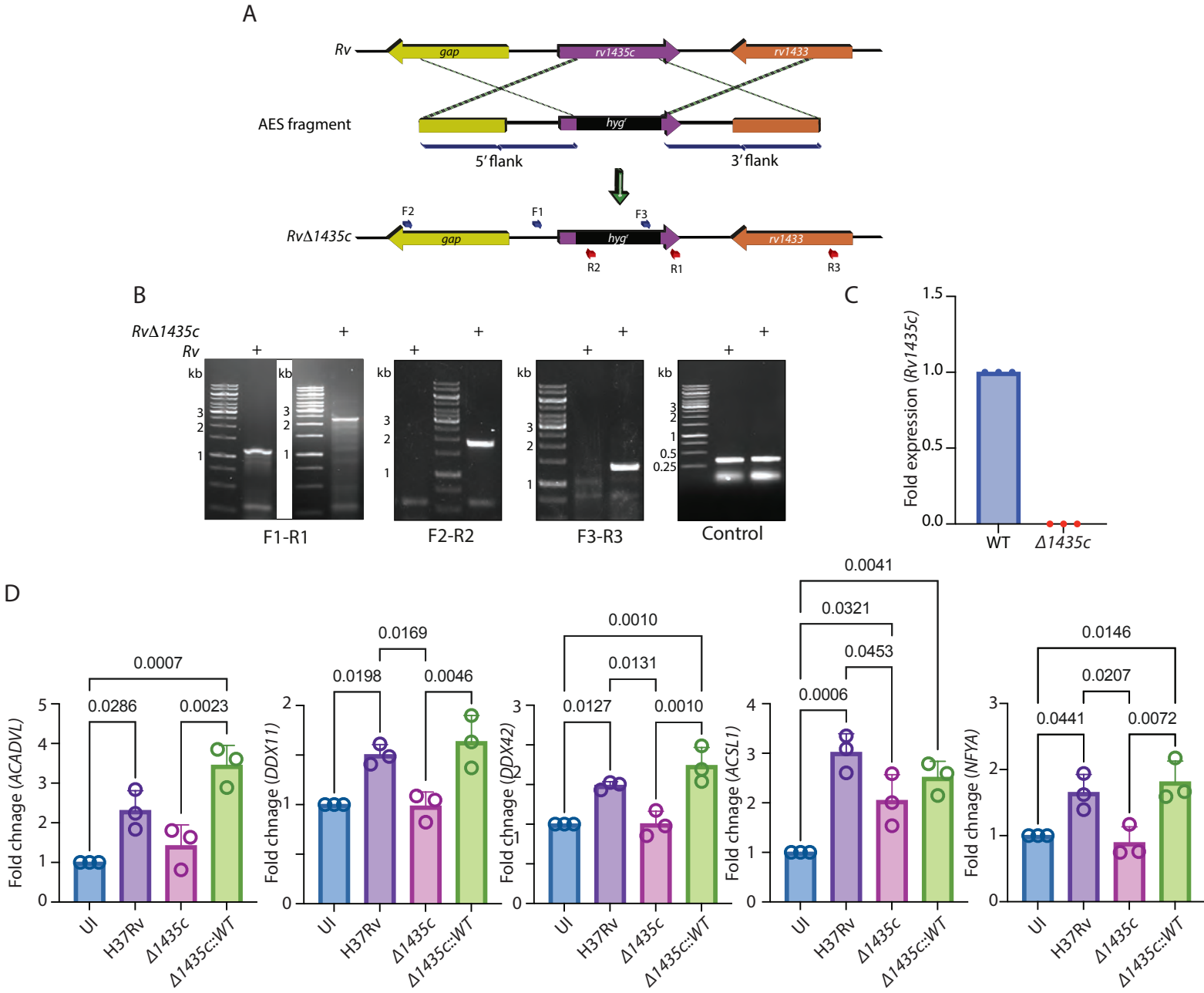
A
Rv
gap
rv1435c
rv1433
AES fragment
hyg'
5' flank
3' flank
RvΔ1435c
F2
F1
F3
R2
R1
R3
B
RvΔ1435c
Rv
kb
F1-R1
F2-R2
F3-R3
Control
C
Fold expression (Rv1435c)
WT
Δ1435c
D
Fold chnage (ACADVL)
Fold chnage (DDX11)
Fold chnage (DDX42)
Fold chnage (ACSL1)
Fold chnage (NFYA)
UI
H37Rv
Δ1435c
Δ1435c::WT
0.0007
0.0286
0.0023
0.0169
0.0198
0.0046
0.0010
0.0131
0.0127
0.0010
0.0041
0.0321
0.0453
0.0006
0.0146
0.0207
0.0441
0.0072

Figure 5

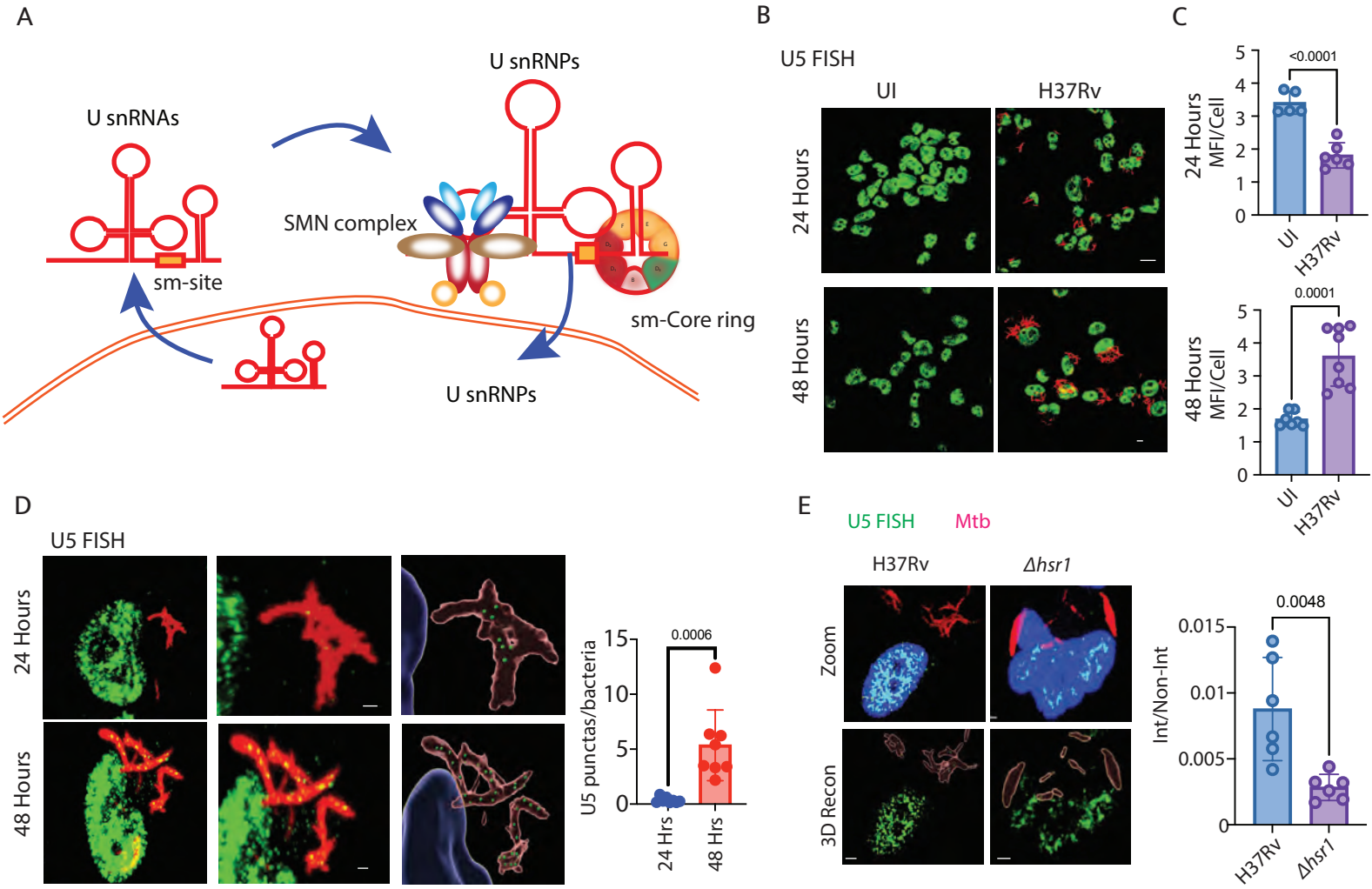
A
U snRNAs
U snRNPs
SMN complex
sm-site
sm-Core ring
U snRNPs
B
U5 FISH
UI
H37Rv
24 Hours
48 Hours
C
<0.0001
24 Hours MFI/Cell
0.0001
48 Hours MFI/Cell
UI
H37Rv
D
U5 FISH
24 Hours
48 Hours
0.0006
U5 punctas/bacteria
24 Hrs
48 Hrs
E
U5 FISH
Mtb
H37Rv
Δhsr1
Zoom
3D Recon
0.0048
Int/Non-Int
H37Rv
Δhsr1

Figure 6

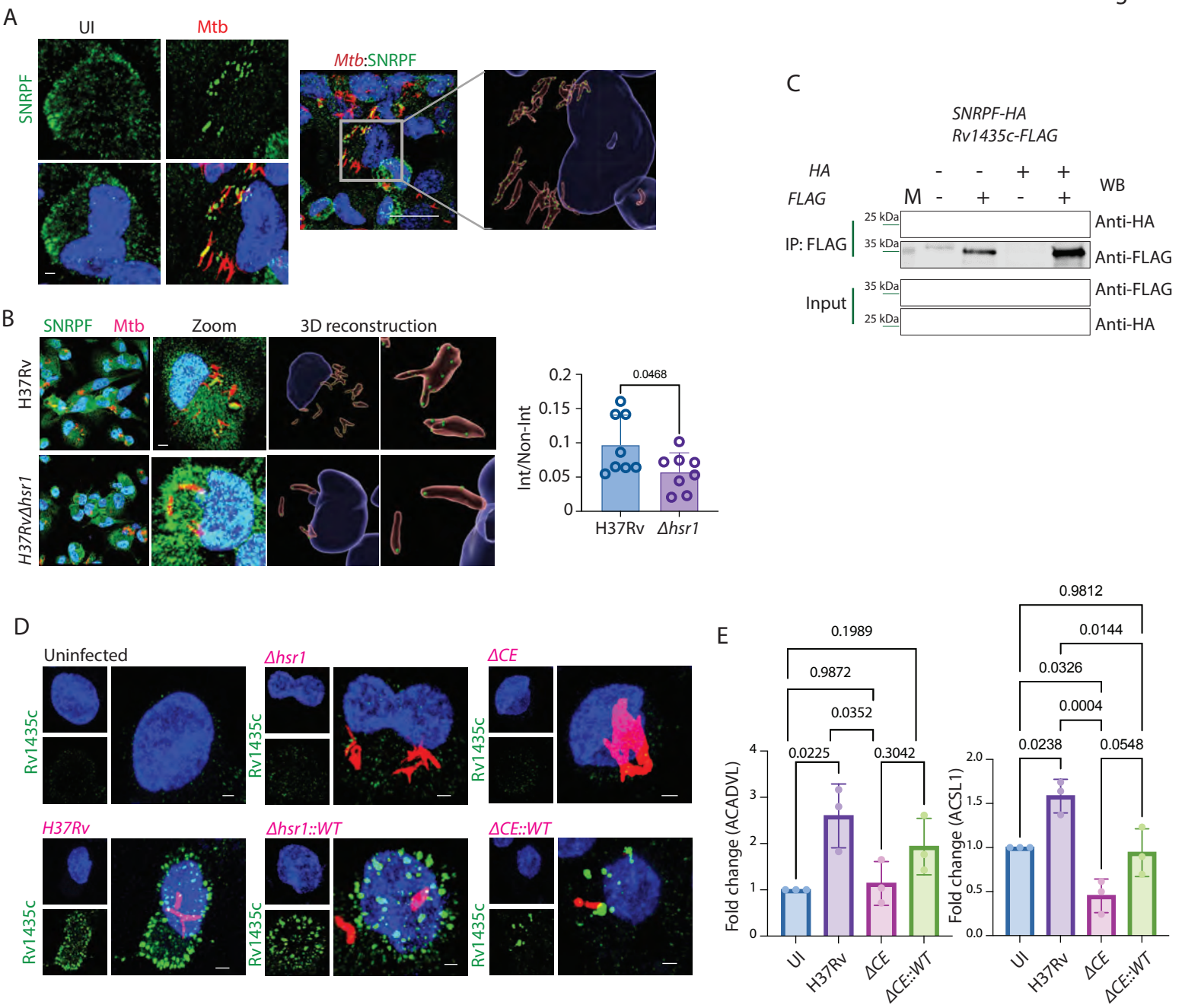
A
UI
Mtb
SNRPF
Mtb:SNRPF
B
SNRPF
Mtb
Zoom
3D reconstruction
H37Rv
H37RvΔhsr1
0.0468
Int/Non-Int
0.2
0.15
0.1
0.05
0
H37Rv
Δhsr1
C
SNRPF-HA
Rv1435c-FLAG
HA
FLAG
M
WB
IP: FLAG
Input
25 kDa
35 kDa
Anti-HA
Anti-FLAG
D
Uninfected
Δhsr1
ΔCE
H37Rv
Δhsr1::WT
ΔCE::WT
Rv1435c
E
0.1989
0.9872
0.0352
0.0225
0.3042
0.9812
0.0144
0.0326
0.0004
0.0238
0.0548
Fold change (ACADVL)
Fold change (ACSL1)
UI
H37Rv
ΔCE
ΔCE::WT

Figure 7

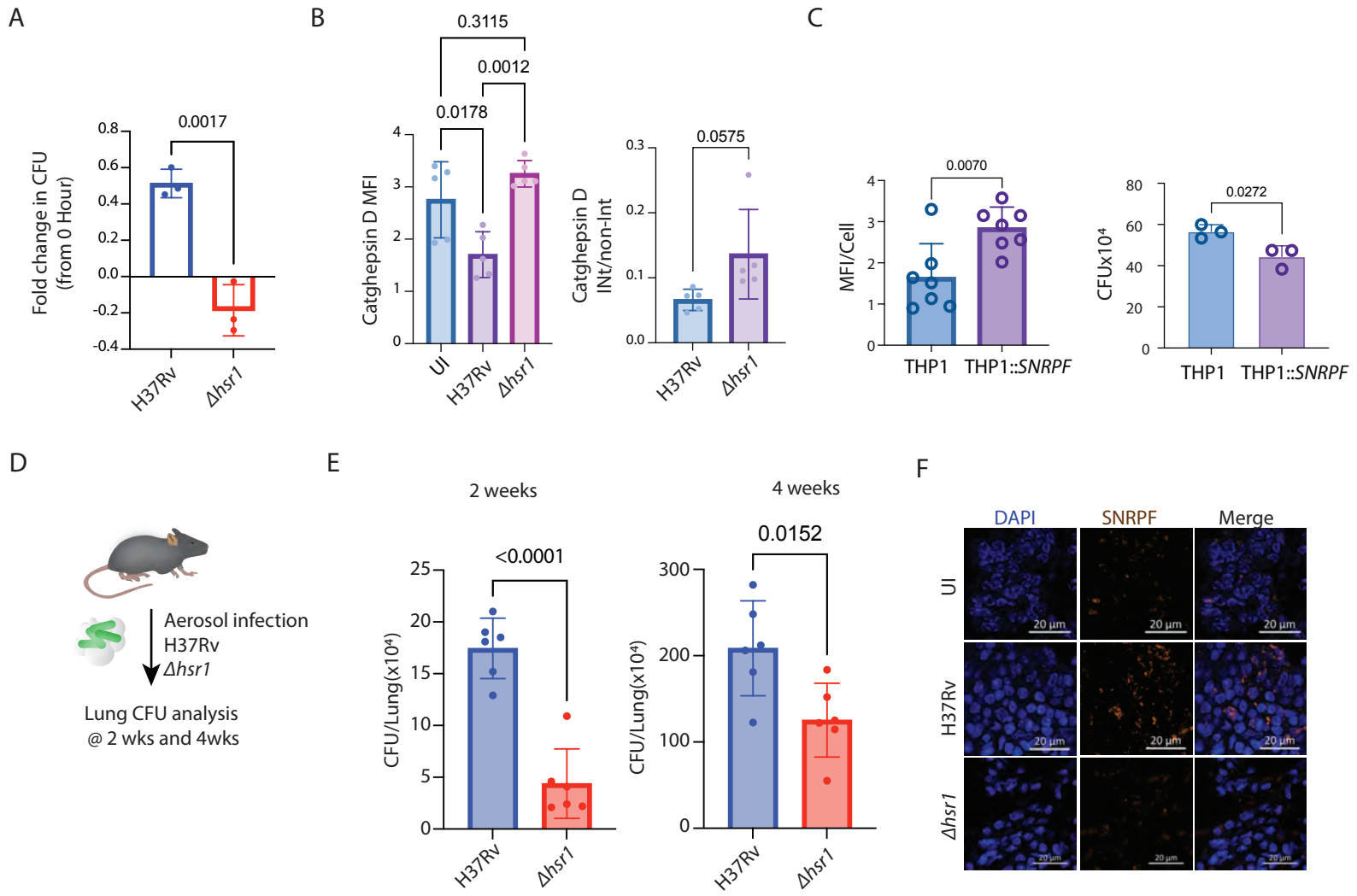
A
Fold change in CFU (from 0 Hour)
0.0017
H37Rv
Δhsr1
B
Catghepsin D MFI
0.3115
0.0012
0.0178
UI
H37Rv
Δhsr1
Catghepsin D INt/non-Int
0.0575
H37Rv
Δhsr1
C
MFI/Cell
0.0070
THP1
THP1::SNRPF
CFUx10⁴
0.0272
THP1
THP1::SNRPF
D
Aerosol infection
H37Rv
Δhsr1
Lung CFU analysis
@ 2 wks and 4wks
E
2 weeks
CFU/Lung(x10⁴)
<0.0001
H37Rv
Δhsr1
4 weeks
CFU/Lung(x10⁴)
0.0152
H37Rv
Δhsr1
F
DAPI
SNRPF
Merge
UI
H37Rv
Δhsr1
20 µm

Figure 8

A

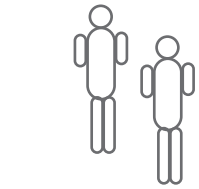

healthy controls (n=19)

PTB (n=20)

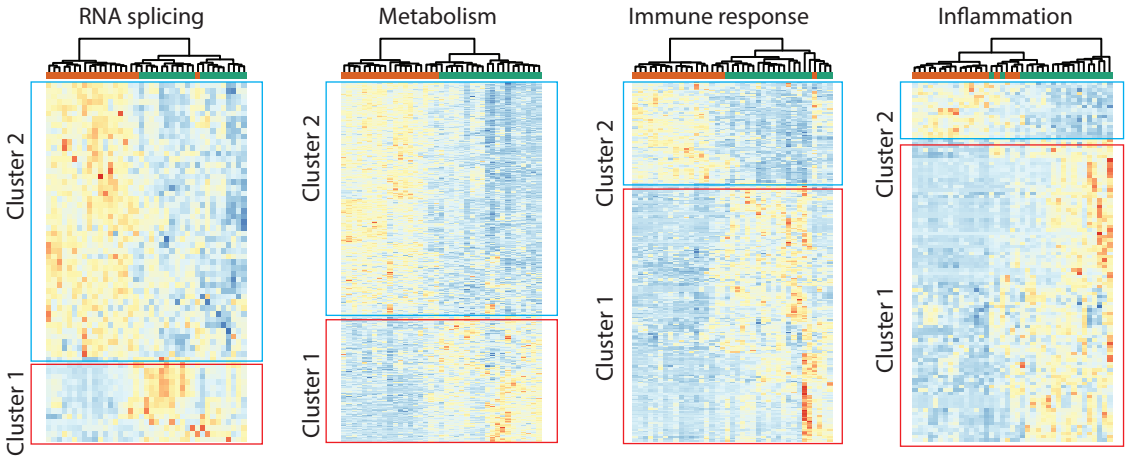

B

SNRPF staining (ITB biopsy)

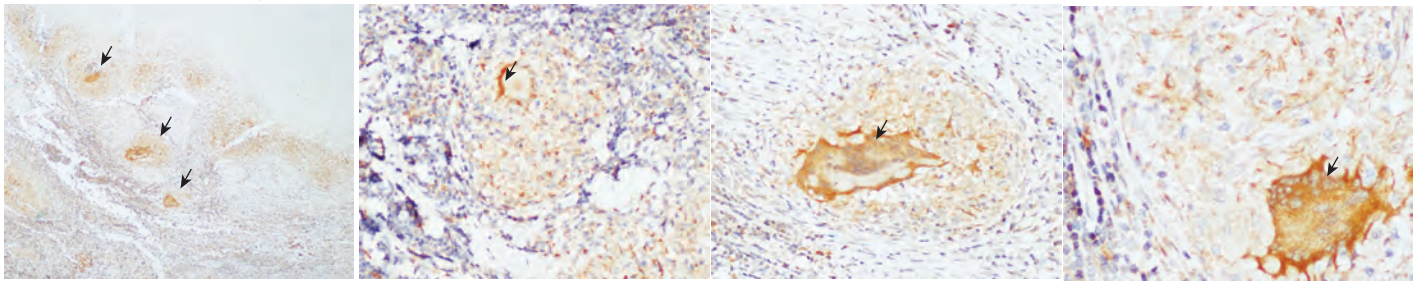

Figure 9

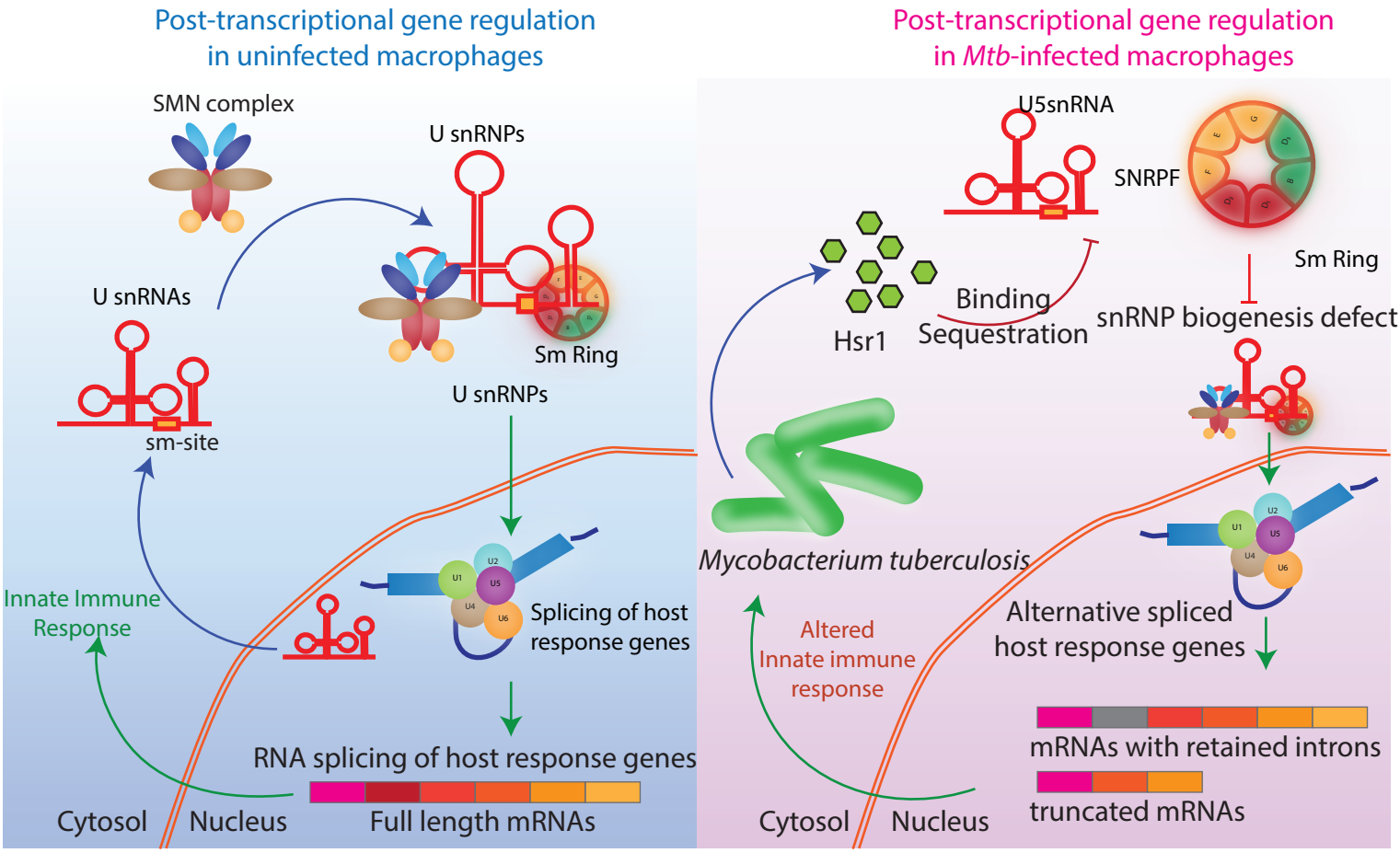
Post-transcriptional gene regulation
in uninfected macrophages
SMN complex
U snRNPs
U snRNAs
Sm Ring
U snRNPs
sm-site
Innate Immune
Response
Splicing of host
response genes
RNA splicing of host response genes
Cytosol
Nucleus
Full length mRNAs
Post-transcriptional gene regulation
in *Mtb*-infected macrophages
U5snRNA
SNRPF
Sm Ring
Hsr1
Binding
Sequestration
snRNP biogenesis defect
Mycobacterium tuberculosis
Altered
Innate immune
response
Alternative spliced
host response genes
mRNAs with retained introns
truncated mRNAs
Cytosol
Nucleus

Supplementary information for the manuscript:

A *Mycobacterium tuberculosis* secreted virulence factor disrupts host snRNP biogenesis

Chauhan, K et al.

Supplementary methods
Supplementary Figures and Legends to Figures S1-S6
Supplementary tables S1-S7

Ethics statement: Studies on human samples were approved by the IEC of AIIMS, New Delhi (Ref no. IEC-304/02-06-2017). For animal experiments, approval was obtained from the Institutional Animal Ethics Committee, ICGEB, New Delhi (ICGEB/IAEC/22092022/CI-28).

Biological materials: Tissue sections from Intestinal TB biopsy samples used in the study were obtained from the Department of Pathology, AIIMS, New Delhi. Access to these materials is subject to institutional guidelines. **Clinical diagnosis of ITB subjects:** The diagnoses depend on clinical features of nocturnal fever, weight loss, diarrhoea, and radiological suspicion of short-segment bowel thickenings, narrowed ileocaecal region, significant mesenteric lymphadenopathy, and/or necrosis. In such cases, an intestinal biopsy is taken, or a segment of the intestine is resected if there is a feature of intestinal obstruction due to fibrosis. All our cases underwent intestinal resection. Histological examination is critical in such cases, and demonstration of large, confluent, multiple, necrotic granulomas with multinucleated giant cells in deeper layers of the intestine are suggestive of ITB, as we have demonstrated in our cases. ZN stain has a very low sensitivity, varying from 5-10%. Such cases are confirmed by either the Gene-Xpert test, Mycobacterial culture, or where such tests are not possible, by ATT trial followed by re-evaluation at two months and six months. All our cases underwent either a *Mycobacterial* culture or a gene-Xpert test.

Antibodies and reagents

The antibodies used in the immunofluorescence experiments were as follows: SNRPD2 (#NBP2-95236), SNRPF(#NBP1-57463), LSm7 (#NBP1-92084), Gemin3 (#NBP2-52454) and Gemin8(#NBP1-83925) from Novus biologicals.DDX23(#A300-693A) from Bethyl Laboratories were used. PKH26 red and PKH67 green fluorescent labelling dyes were used from Sigma-Aldrich. The spliceosome complex pull-down was done using an anti-SNRPB antibody (Y-12, MA513449). The antibodies used in immune-blotting experiments were as

34 tubulin (Abcam plc; ab6046), histone (Abcam plc; ab18521), IRDye 800CW Goat anti-mouse
35 IgG secondary antibody (LI-COR Biosciences)and IRDye 680RD goat anti-rabbit IgG
36 secondary antibody(LI-COR Biosciences). The co-immunoprecipitation was done using
37 EZView Red Anti-HA affinity gel (E6779), Anti-FLAG M2 Affinity gel (A2220) and
38 immunoblots were detected using Anti-HA antibody, Mouse monoclonal (H3663) and
39 Monoclonal Anti-FLAG M2 antibody mouse (F1804) from Sigma-Aldrich.

40 **Cell culture**

41 Mammalian cells: THP1 monocytes (ATCC) were maintained in RPMI 1640 media (Cell
42 Clone), and HEK293T cells (ATCC) were maintained in DMEM media (Cell Clone). Cells
43 were grown at 37°C with a 5% CO2 atmosphere. All the media was supplemented with 10%
44 fetal bovine serum. HEK293T cells were transfected with plasmids at a 30-50% confluency
45 using jetPRIME buffer (Polyplus #712-60) as per manufacturer protocol. The siRNA was
46 transfected using the Dharmafect reagent. HEK293T constitutively expressing PRINT plasmid
47 was selected in the presence of blasticidin (Gibco) 20 µg/ml concentration.
48 Bacterial Cells: *M. tuberculosis H37Rv*, *M. smegmatis* mc^2155 and mutant strains were grown
49 at 37°C to log phase in Middlebrook 7H9 media with 0.05% Tween80, 10% ADC Enrichment,
50 and 0.2% glycerol. Plasmids were selected with 50 mg/ml kanamycin or hygromycin
51 depending upon the resistance marker.
52 **Infection**
53 THP-1 cells were activated into macrophages by treatment with 32 nM PMA (Sigma) for 24
54 hours, followed by another 24 hours for recovery. The THP-1-derived macrophages were
55 infected with *Mtb* strains at an MOI of 10 for 4 hours, followed by 2 hours of amikacin (200
56 µg/µl) treatment. *M. smegmatis* infection was performed at an MOI of 10 for 1 hour, followed
57 by 2 hours of amikacin treatment. Amikacin treatment clears all the extracellular bacteria,
58 which are washed following the treatment, and this time point is considered as 0 hours of
59 infection throughout the manuscript.

60 **RNA isolation and qPCR**

61 RNA was isolated at indicated time points using MDI mammalian Total RNA isolation kit
62 (MTRK250) as per the manufacturer's protocol. The RNA was quantified using a nanodrop
63 spectrophotometer. 1000ng RNA was used to make cDNA using the Iscript cDNA synthesis
64 kit (BioRad #170-8891), and 2 µl of 1:5 diluted cDNA was used to set qPCR on the BioRad

65 CFX384 well plate qPCR machine. Primers were custom synthesized from Sigma Aldrich
66 Chemicals Ltd. A list of primers used in this study is provided in the table S7.

67 **Transformation of yeast cell**

68 The yeast competent cells were prepared by harvesting yeast cells by centrifugation at 400 rpm
69 for 5 min at 25 °C. The supernatant was discarded, and the pellet was washed and resuspended
70 in filter-sterilized SORB buffer (100 mM Lithium acetate, 100 mM Tris HCl, pH 8.0, 1 mM
71 EDTA, pH 8.0, 1 M sorbitol pH 8.0) to which denatured salmon sperm DNA was added (10
72 mg/ml). The bait (pGBDKT7 vector) plasmids were mixed gently with the Y187 competent
73 cells. Then PEG mixture was added and incubated at 30 °C for 30 min, 42 °C for 30 min and
74 4 °C for 30 min in a thermocycler machine. Tubes were taken out and plated on 15 cm diameter
75 SC-TRP plates (Cat No. Clonetech 630413). Plates were incubated at 30°C for 2 to 7 days. A
76 similar protocol was used for the prey (pGADT7 vector) plasmid in the AH109 yeast strain on
77 SC-Leu medium (Cat No. Clonetech 630414).

78 **Y2H assay between bait and prey libraries**

79 The bait library was prepared by plating the Y187 yeast strain (bait) transformed with Mtb
80 proteins in 384 well patterns on the Singer Robot Plate. The AH109 (prey) yeast strain
81 transformed with host spliceosome protein was grown in SC-leu broth medium and equally
82 plated on a robotic compatible square plate. Using 384 pinned robotic pad bait libraries were
83 patched on another YAPD plate. Each plate was then patched with individual cells containing
84 prey plasmid and mixed well using the robotic system. This step was performed 4 times as four
85 independent mating steps, thereby making it a total of 1536 spots per plate. The plate containing
86 mixed colonies was kept for mating of both strains at 30 °C for 36 hours. After 36 hours these
87 colonies were selected on SC-Trp-Leu (Cat No. Clonetech 630417) plates for the selection of
88 those cells which contain both plasmids (bait as well as prey). After 72 hours these plates were
89 replicated on SC-Trp-Leu-His (3 drops-out, Clonejet 630419) and SC-Trp-Leu-His-Ade (4
90 drop-outs, Clonetech 630428) for the screening of interaction between the protein which was
91 fused with bait and prey respectively. The colonies that appear on both 3-DO and 4-DO plates
92 represented very specific and strong interactions between the bait and prey proteins.

93 **Co-immunoprecipitation and Immunoblotting**

94 The cells were lysed using a non-denaturing IP lysis Buffer (20 mM Tris-Cl, 137 mM NaCl, 2
95 mM EDTA, 10% glycerol, 1% NP-40, pH 8) and centrifuged at 14000 rpm for 10 min at 4 °C.

96 The supernatant was precleared using IgG beads, and 300 µg of protein was used for IP. The
97 IP was performed using FLAG-tagged beads (Sigma) and HA-tagged beads (Sigma) at 4 °C
98 for 4 hours, followed by three washes with IP buffer. The beads were then boiled in 2X SDS
99 loading dye. The protein samples were subjected to SDS PAGE followed by transfer on
100 nitrocellulose membrane (BioRad) using BioRad Turbo transfer blot. The blocking was
101 performed by Odessey blocking buffer (LI-COR Biosciences) in 1:1 dilution with 1X PBS at
102 room temperature. The blots were immunoblotted with primary antibodies, followed by IR-
103 tagged secondary antibodies (LI-COR Biosciences). Blot imaging was done using Odessey IR
104 Imaging System (LI-COR Biosciences).

105 **Immunofluorescence**

106 For immunofluorescence experiments, ~0.2x 10^6 cells were plated on 12 mm coverslips per
107 well in a 24- well plate. Cells were infected with m-cherry expressing *Mtb*, and other strains
108 were labelled with PKH67 fluorescent dye (Sigma). The cells were fixed using 4% v/v
109 paraformaldehyde for 20 min at room temperature for indicated time points. The cells were
110 incubated with blocking buffer (0.02% Triton-X100, 3% w/v BSA in 1XPBS) for 1 hour. The
111 cells were washed thrice with 1X PBST and incubated with primary antibodies for 3 hours.
112 The cells were washed thrice with 1XPBST and incubated with secondary Alexa Flour (488,
113 555, 590 or 670nm) tagged antibodies (Invitrogen). The nucleus was stained using DAPI (300
114 nM) for 10 min. The cells were mounted on slides with Pro-Long Gold antifade reagents (Life
115 Technologies). All the incubation and staining were done at room temperature. Images were
116 acquired by NIS-Elements software using the Nikon A1R laser scanning confocal microscope
117 equipped with a Nikon Plan Apo VC ×20, NA 0.75, and Plan Apo VC ×100 oil, NA 1.40
118 objectives were used. Serial confocal sections, 0.5 µm thick, were acquired with a z-stack
119 spanning 10–15 µm to form a composite image. Images were analysed using Imaris 9.6.6
120 imaging software using several tools like deconvolution, 3D-reconstruction and shortest
121 distance calculation amongst others, NIS-Elements and image J software.

122 **Fluorescent reporter splicing assay using flow cytometry**

123 For Flow cytometry experiments, ~0.5 x 10^6 HEK293T cells constitutively expressing pRINT
124 vector (Addgene plasmid # 24218) were plated on 12 well plates. These were co-transfected
125 with 800ng of modified pGINT vector (Addgene plasmid # 24217) with exon skipping cassette
126 and *Mtb* protein-expressing vectors at a ratio of 1:1 using jetPRIME buffer. The cells were
127 fixed using 4% v/v paraformaldehyde in 1X PBS for 20 minutes at room temperature. Then,

128 the cells were scraped and resuspended in 1X PBS. The data were acquired using BD
129 FACSDiva acquisition software in BD FACS Fortussa cytometer (BD).

130 **Spliceosome complex Co-IP**

131 For the pulldown experiment, ~200 million THP-1 derived macrophages were infected with
132 H37Rv at an MOI of 10 and samples were processed 48-hour post-infection. The nuclear and
133 cytoplasmic extract was prepared using the Active Motif Nuclear Complex Co-IP kit
134 (catalogue No.54001) per the manufacturer's guidelines. The nuclear extract and cytoplasmic
135 extract were passed through a 0.2-micron filter. 500 µg of nuclear extract and cytoplasmic
136 extracts were used for pulldown using 10 µg Y-12 antibody (MA5-13449, Thermo Fisher) or
137 IgG-control (Sigma) antibody for each condition. The Y-12 antibody was crosslinked using
138 DMP (20 mM) to Protein A-Sepharose beads for 1 hour (beads were washed prior with 0.2 M
139 sodium borate, pH 9.0) followed by 0.2 M ethanolamine incubation for 1 hour at room
140 temperature. The Nuclear and Cytosolic extracts were then incubated with crosslinked beads
141 overnight at 4 °C. The beads were washed thrice with wash buffer (0.025 M Tris, 0.15 M NaCl,
142 pH 7.2). The protein was finally eluted in 50 µl of an elution buffer containing primary amine
143 pH 2.8. To neutralize the low pH of the elution buffer, 1 M Tris (pH 9.5) was added to the
144 collection tube.
145

146 **Mass Spectrometric Data analysis for immune-precipitated spliceosome complex**
147 *Sample Preparation*- An equal volume of eluted protein sample (50ul) was used for digestion
148 and reduced with 5 mM TCEP and further alkylated with 50 mM iodoacetamide and then
149 digested with Trypsin (1:50, Trypsin/lysate ratio) for 16 h at 37 °C. Digests were cleaned using
150 a C18 silica cartridge to remove the salt and dried using a speed vac. The dried pellet was
151 resuspended in buffer A (2% acetonitrile, 0.1% formic acid). An equal amount of peptide (1ug)
152 was injected into the analytical column. *Mass Spectrometric Analysis of Peptide Mixtures*- All
153 the experiments were performed using EASY-nLC 1000 system (Thermo Fisher Scientific)
154 coupled to Thermo Fisher-QExactive plus equipped with nano electrospray ion source. 1ug
155 peptide was loaded on C18 column 50 cm, 3.0µm Easy-spray column (Thermo Fisher
156 Scientific) at column heating temp 40 C. Peptides were eluted with a 0–40% gradient of buffer
157 B (80% acetonitrile, 0.1% formic acid) at a flow rate of 300 nl/min) and injected for MS
158 analysis. LC gradients were run for 90 minutes MS1 spectra were acquired in the Orbitrap
159 (Max IT = 50ms, AGC target = 3e6; R=70K, mass range = 350-1750; Profile data). Dynamic
160 exclusion was employed for 30s excluding all charge states for a given precursor. MS2 spectra

161 were collected for top 15 peptides. MS2 (Max IT= 100ms, R= 17.5K, AGC target 1e5). *Data*
162 *Processing*- All samples were processed and RAW files generated were analysed with
163 Proteome Discoverer (v2.2) against the Uniprot Human and Mtb database. For dual Sequest
164 and Amanda search, the precursor and fragment mass tolerances were set at 10 ppm and 0.5
165 Da, respectively. The protease used to generate peptides, i.e. enzyme specificity was set for
166 trypsin/P (cleavage at the C terminus of "K/R: unless followed by "P"). Carbamidomethyl on
167 cysteine as fixed modification and oxidation of methionine, N-terminal acetylation were
168 considered as variable modifications for database search. Both peptide spectrum match and
169 protein false discovery rate were set to 0.01 FDR. Only statistically significant proteins (Using
170 ANNOVA p-value cut off 0.05) that were found in all three biological replicates across and in
171 all experimental groups were used to generate heatmap and for further analysis.

172 **RNA FISH**

173 RNA-fluorescence *in situ* hybridization (RNA FISH) was performed using previously
174 described snRNA probes [1]. The sequences of the oligonucleotide used for FISH were as
175 follows: U5 snRNA, 5′-CTC TCC ACG GAA ATC TTT AGT AAA AGG CGA AAG ATT
176 TAT ACG ATT TGA AGA G-3′; The U5 snRNA probes were labelled with Alexa Flour 647
177 (Invitrogen) at their 5' end. Next, the cells were fixed with 4% v/v paraformaldehyde for 20
178 min at room temperature. Next, cells were permeabilized and incubated with RNA-FISH probe
179 for three hours at 40 °C by using the ViewRNA™ ISH Cell Assay Kit system (Thermo
180 Fischer). Subsequently, cells were immune-stained and mounted using a Pro-Long gold
181 antifade (Life technologies).

182 **Bacterial transformations**

183 For the generation of *M. smegmatis* mutants expressing *H37Rv* proteins, 50 ml of an early
184 exponential phase culture of *M. smegmatis* mc^2155 was washed twice and concentrated ice-
185 cold 10% ultrapure glycerol (Invitrogen). Concentrated cells were electroporated with
186 approximately 10 µg of pNit plasmid. Electroporation was carried out at 2500 V, 25 µF, and
187 1000 Ω in the Biorad gene pulsar. Electroporated cells were allowed to recover at 37 °C in 7H9
188 Middlebrook broth and plated on 7H11 supplemented with 10% OADC and kanamycin (25
189 µg/ml; Sigma).

190 ***Mtb* survival assay**

191 For CFU experiments, ~0.01 million THP-1 macrophages were seeded in a 96-well plate and
192 *Mtb* infection was done at an MOI of 10. The lysis was done by incubating with 0.06% SDS
193 for 5 min at indicated time points. The lysed cells were diluted to 1:10 and 1:50 in 7H9 media
194 and 10 µl of the dilutions were plated in a drop-wise fashion on a 7H11 plate supplemented
195 with 10% OADC. The plates were incubated for approximately around 3 weeks for colony
196 enumeration at 37 °C.

197 **Expression and purification of recombinant proteins**

198 The Mtb proteins were cloned in the pEZY19 vector and transformed into E. coli BL21(DE3)
199 competent. Protein expression was induced with 0.1 mM isopropyl b-D-1-
200 thiogalactopyranoside (IPTG) for 16-19 hours. Collected frozen cells were lysed in a lysis
201 Buffer (50 mM Tris-HCl pH. 8.0 containing 300 mM NaCl,10% Glycerol, 1mm DTT, 1mm
202 PMSF,1mm BHCL,0.1% Triton X-100, 10mM imidazole and lysozyme 1mg/ml) followed by
203 sonication (0.5 s pulse and 0.9 s rest) at 2 min intervals to prevent overheating. After
204 centrifugation, the proteins were purified from the supernatant using nickel-nitrilotriacetic acid
205 (Ni-NTA) affinity chromatography (Cat. No.- 30410, Sigma). The recombinant proteins were
206 eluted from Ni-NTA resins by elution buffer (50 mM Tris-HCl pH. 8.0 and 300 mM NaCl)
207 containing 300mm Imidazole. The purified protein was concentrated using 10Kda Centricon
208 (ACS501024, Millipore) subjected to gel permeation chromatography on GE Healthcare
209 Superdex 75 Increase 10/300 GL where the monomeric fraction of the protein was eluted. The
210 final protein was stored in 50 mM Tris-HCl pH. 8.0 containing 300 mM NaCl,10% Glycerol
211 buffer at -80˚C.
212

213 **BALB/c aerosol challenge**

214 All mice experiments were carried out in the Tuberculosis Aerosol Challenge Facility (TACF,
215 ICGEB, New Delhi, India). BALB/c mice have been housed in individually ventilated cages
216 contained within the biosafety level 3 enclosure. The animal holding area of the BSL3 lab is
217 maintained at 20–25 °C, 30–60% humidity and 12–12 h of the light–dark cycle. An aerosol
218 challenge of ~100 CFUs was given to the animals in a Wisconsin–Madison chamber according
219 to the standardized protocol in the TACF facility. Two animals were selected randomly and
220 humanely euthanized 24 h post aerosol challenge to check for infection establishment. The
221 lungs and spleen tissues were harvested and homogenized to enumerate CFU. Tissue lysates

222 were serially diluted and plated on Petri plates containing Middlebrook 7H11 agar (Difco)
223 supplemented with 10% OADC (Becton, Dickinson) and 0.5% glycerol.
224
225 **RNA-Seq analysis**
226 Reads were quality filtered using Trimmomatic (v.0.39, LEADING:10 TRAILING:10
227 SLIDING WINDOW:4:15 MINLEN:75) [2] and were assessed for quality using FastQC (v.10.1)
228 [3] and visualised with MultiQC (v.1.9)[4]. Salmon (v.1.8, –numGibbsSamples 30) [5] was used to
229 quantify quality filtered reads against the human genome (GRCh38, primary assembly) with
230 Gencode annotation (v.40) [6]. Profiles were imported using tximeta (v.1.10) [7] and [8] (v.1.22) and
231 filtered to retain all transcripts from only protein-coding genes. Statistical analysis was done
232 using swish methodology from fishpond (v.1.8) [9] and significantly differentially expressed
233 transcripts (DETs) were defined based on *qvalue* ≤ 0.1. Furthermore, Isoform usage was
234 analysed using IsoformSwitchAnalyzeR (v.1.18) [10] with reduceToSwitchingGenes = FALSE,
235 reduceFurtherToGenesWithConsequencePotential = FALSE, No dIFcutoff and Isoform
236 fraction cuffoff. Heatmap of the DETs was generated with [11] using mean z-scaled normalised
237 scaled TPM values and clustered based on Euclidean distance and Ward.D2 methodology.
238 Clusters were defined manually. Enrichment analysis was done separately on overexpressed
239 and repressed DETs from each pairwise comparisons using enrichR (v.3.0) [12] with KEGG
240 Human 2021 and Gene Ontology (GO) [13] (Biological Process (BP), Cellular Component (CC)
241 and Molecular Function (MF)) 2021 database figures were generated using ggplot2 (v.3.3.5)
242 [14]. Analyses were done in R statistical software environment (v.4.1) [15].
243
244 **Generation of Rv1435c mutant**
245 *Rv1435c* mutant was generated using recombineering methodology which requires an Allelic
246 exchange substrate [16]. To construct that, 836bp upstream (LHS) and 1Kb downstream (RHS)
247 regions of the *Rv1435c* locus (retaining ~170 bp of the gene at both ends) were amplified from
248 *Mtb* (*H37Rv* genome) with the help of primers having appropriate restriction endonuclease sites
249 (LHS-DraIII; RHS-SfiI). The flanks were then digested and ligated with other two fragments-
250 Hygromycin resistant cassette and *oriE*+cosλ with compatible ends to create a four-piece AES.
251 The latter was then digested with SnaBI sites to release the linearised fragment consisting of
252 LHS-*Hyg*^{r}-RHS and electroporated into recombineering proficient *Rv::pNitET* (Kan^r) strain
253 that overexpresses RecET recombinases upon over-expression using Isovaleronitrile. Mutant
254 colonies were analysed using different primer sets to confirm legitimate recombination at the

255 required locus and cured of the pNitET plasmid by negative selection on 2% sucrose-containing
256 7H11-hyg^r agar plates.
257
258 Primers used:
259 *Rv1435c* 5' Flank forward primer with DraIII & SnaBI site:
260 5'CACCTTTTCACAAAGTGTACGTACGTGGTGCACGACGCATTGGA 3'
261 *Rv1435c* 5' Flank reverse primer with DraIII site:
262 5' TTTTTTTTCACTTCGTGCGCCGGCGGCTACCGGCGCGT 3'
263 *Rv1435c* 3' Flank forward primer with SfiI site:
264 5' CACCTTTTGGCCTAGATGGCCGGGCCGGTCCTGGCTGGTGCT 3'
265 *rv1435c* 3' Flank reverse primer with SfiI site and SnaB1 site:
266 5' TTTTTTTTGGCCACTTAGGCCTACGTAGGGATCGCTGGGAGCGTGGTT 3'
267
268 **Generation of Rv1435c complementation construct pSCW-F-Rv1435c**
269 *Rv1435c* was cloned along with its native promoter (500bp upstream of the gene) between ScaI
270 and HindIII sites using an integrative vector, pSCW-F (C-terminal 3X FLAG tag), which
271 facilitates the integration of the gene at Tweety attP sites in the *Mtb* genome.
272 Primers used:
273 FP *Rv1435c* (with UPSTREAM 500bp) ScaI
274 5' FP : 5' CACCAGTACTATGCGCCAGCGTGCTGTTG 3'
275 RP *Rv1435c* HindIII, w/o stop codon
276 5'TTTTAAGCTTGCGCGCACCTGCGGGC 3'
277
278 **Immunohistochemical staining:** The paraffin-embedded specimens were cut into 4–5 µm-
279 thick sections, deparaffinized in xylene for 5–10 min, and dehydrated through a series of graded
280 alcohols (100%, 100%, 95% and 80%). Tissue sections were boiled at 100°C for 30 min in
281 10mM citrate buffer (pH 6.0), followed by cooling and treatment with blocking solution (100%
282 methanol containing 0.3% H_2O_2) for 30 min to block any endogenous peroxidase activity. They
283 were incubated with SNRPF or SNRPD2 primary antibody (1:600, pH 9) overnight at 4°C,
284 followed by incubation with secondary antibody (Ultra trek anti polyvalent kit with HRP
285 conjugated secondary kit, Scy Tek Laboratories, Logan, USA) for 30 mins at room
286 temperature. The slides were thereafter stained with 3,3′-Diaminobenzidine (DAB). Finally,
287 the sections were counterstained with Hematoxylin and Eosin and observed under a
288 microscope. **Interpretation of IHC results:** SNRPF staining in >10% of cells was considered

289 positive. Both cytoplasmic and nuclear staining were looked for. The spatial distribution of the
290 stained sections, in terms of granulomas areas and areas away from granulomas, were noted
291 down to identify polarization of staining, if any.
292

Legends to Figures S1-S9:

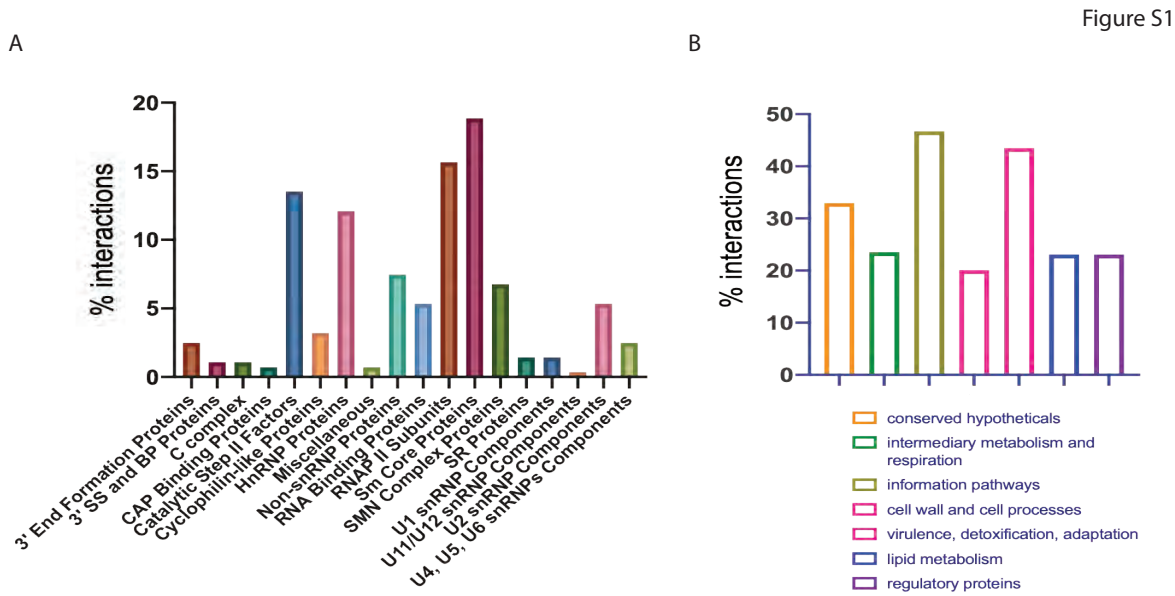

Figure S1: Mycobacterial secretory proteins and host spliceosome proteins interactome.

A) The percentage of the interaction shown by spliceosome-related proteins belonging to different spliceosome protein categories

B) The percentage of the interacting Mtb proteins belonging to the different functional classifications.

Figure S2

Gene	No. of isoform in Y2H	Interacting transcript	Interaction
SNRP40	2	0	No
PQBP1	2	0	No
NCBP2	2	0	No
POLR2H	4	4	19/10/4/1
SF3B1	2	0	No
SYF2	2	2	2 (Rv1643, Rv2927c)
DCAF4	2	1	2 (Rv1643, Rv2927c)
SNRPD2	2	1	16 (Rv1643, Rv2927c, Rv1566c)
LSm7	2	1	26 (Rv3864, Rv1643, Rv2927c, Rv1566c)
LSm4	2	0	No
SNRPG	3	0	No
RBPMS	2	0	No
SF1	3	0	No
CSTF	2	0	No
LUC7L2	2	1	4 (Rv1643, Rv2927c)
RBMX	2	1	8 (Rv3849)
U2AF1	3	1	2 (Rv1643, Rv2927c)
PPIH	3	1	1

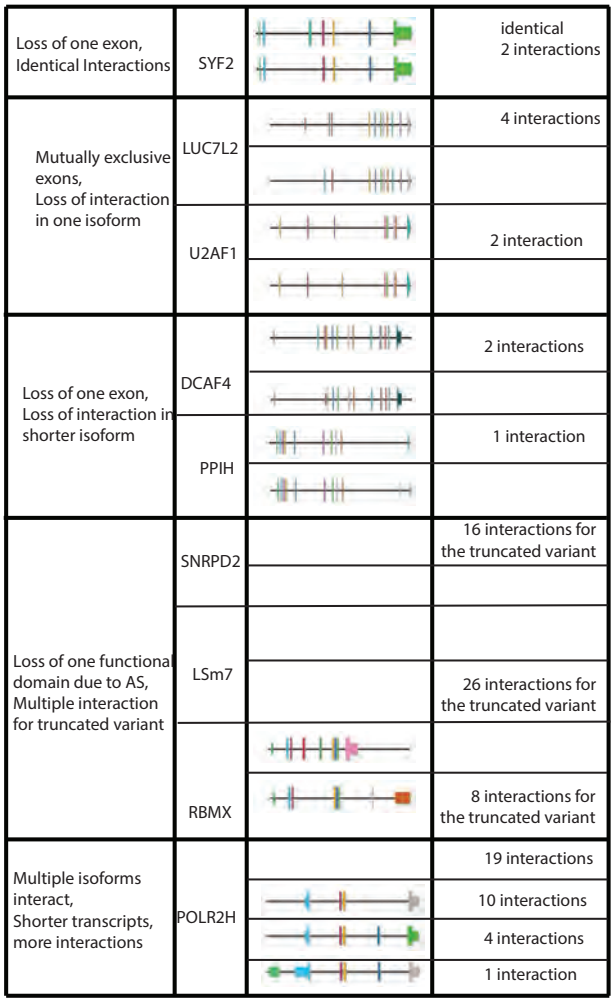

Figure S2: Interaction of Mtb proteins with the splice variants of human proteins.

A) A descriptive list of the human spliceosome proteins, represented by more than one isoform in the AD library, along with their interactions with the *Mtb* protein, is presented in the table.

B) The table shows the distinct spliced mRNA isoforms that are classified as loss of exon, mutually exclusive exon and loss of the functional domain. The isoforms of SYF2, differing by only one exon, show interaction with the same *Mtb* proteins, suggesting no contribution of alternatively spliced exons towards interaction. Only one of the isoforms of genes which show exon skipping, like DCAF4 and PPIH, or mutually exclusive exons like U2AF1 and LUC7L2, showed interaction with any *Mtb* proteins, suggesting the involvement of alternative exons in the interactions. The truncated isoforms of SNRPD2, LSm7 and RBMX show a loss of functional domains and multiple interactions with Mtb proteins, while the longer isoforms for these genes did not show any interactions. Similarly, the truncated isoforms of POLR2H show more interaction.

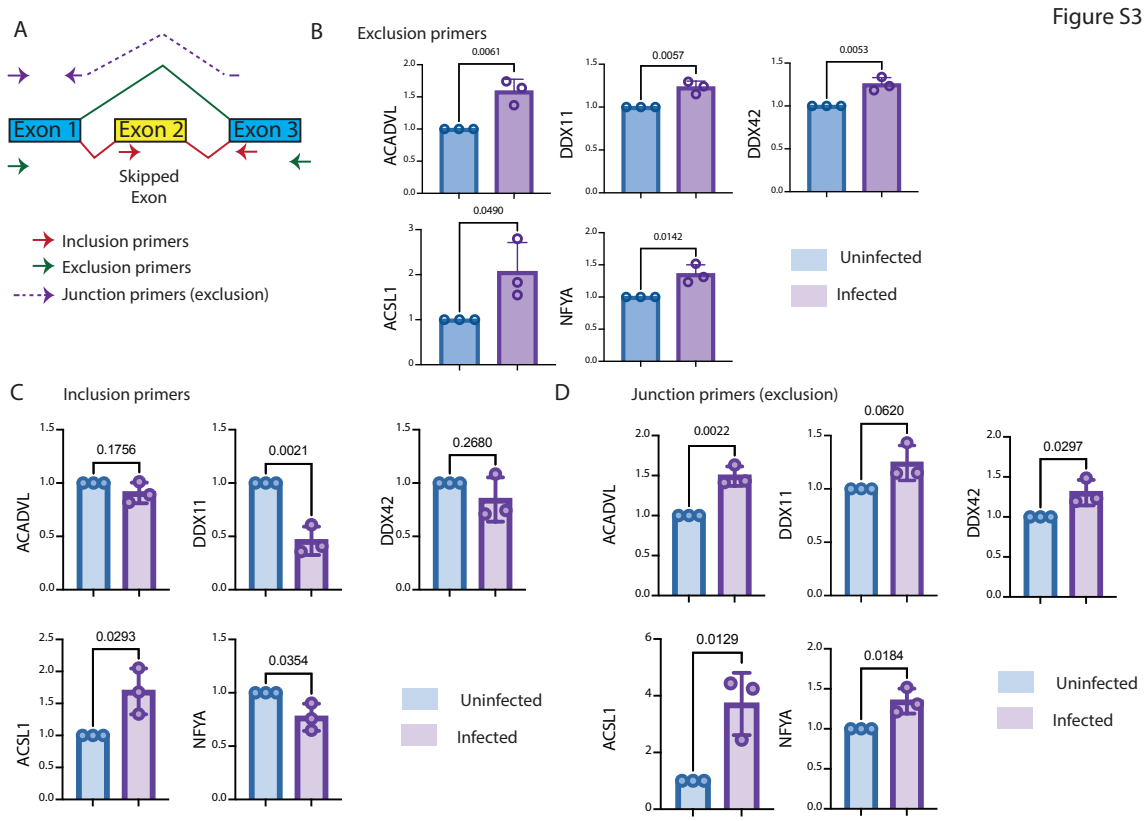

Figure S3: Altered RNA splicing in *Mtb*-infected THP-1 macrophages

A) The schematic shows the primer design strategy for exon-inclusion, exon-exclusion and exon-junction primers.

B) Expression of five target genes (as indicated) in THP-1 macrophages upon infection with H37Rv using exon exclusion primers at 48 hpi. Data from three independent biological experiments.

C) Expression of five target genes (as indicated) in THP-1 macrophages upon infection with H37Rv using exon inclusion primers at 48 hpi. Data from three independent biological experiments.

D) Expression of five target genes (as indicated) in THP-1 macrophages upon infection with H37Rv using exon junction primers at 48 hpi. Data from three independent biological experiments.

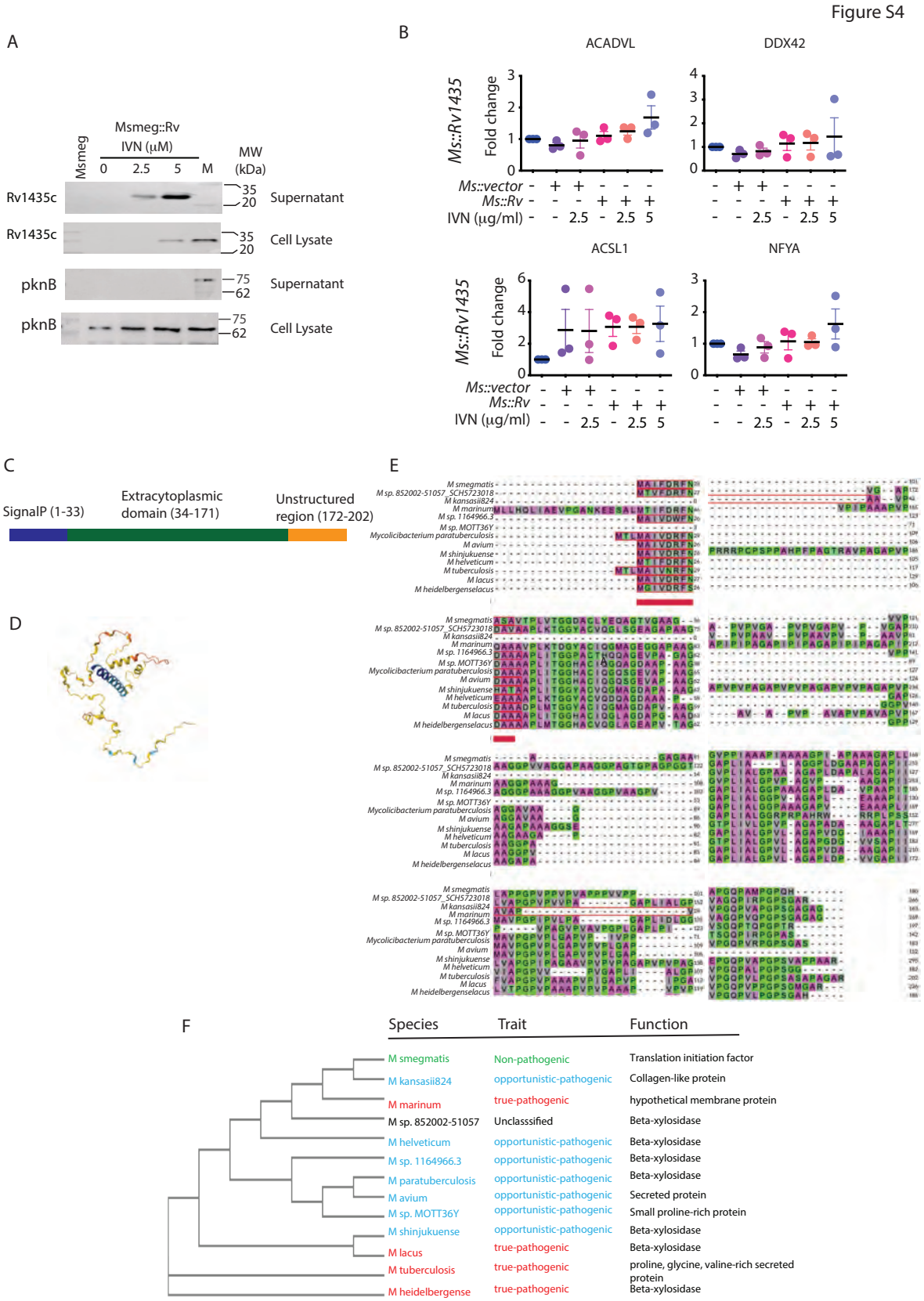

Figure S4: Rv1435 secretion from the modified *M.smegmatis* strains

A) The protein expression in modified *M. smegmatis* strains expressing Rv1435c upon induction with 2.5μM and 5 μM IVN was checked by immunoblotting in

whole cell lysate and culture supernatant (SN). As control, the modified *M. smegmatis* strains expressing pknB were also induced with IVN and its expression in the supernatant or whole cell lysate was measured by immunoblotting.

B) Isoform-specific qPCR to assess the impact of Rv1435c expressing *Msmeg* infection in THP-1 macrophages on exon skipping event in *ACADVL*, *DDX42*, *ACSL1* and *NFYA*; N=3, indicating p values from One-way ANOVA.

C) Domain organization of Rv1435c depicting signalP, extracytoplasmic and disordered regions.

D) Predicted structure of Rv1435c from AlphaFold Protein Structure Database

E) Multiple sequence alignment of Rv1435c protein in different mycobacterial species using CLUSTAL Omega. The red bar indicates the conserved sequence among different species.

F) A phylogenetic tree corresponding to the multiple sequence alignment is shown in S6C.

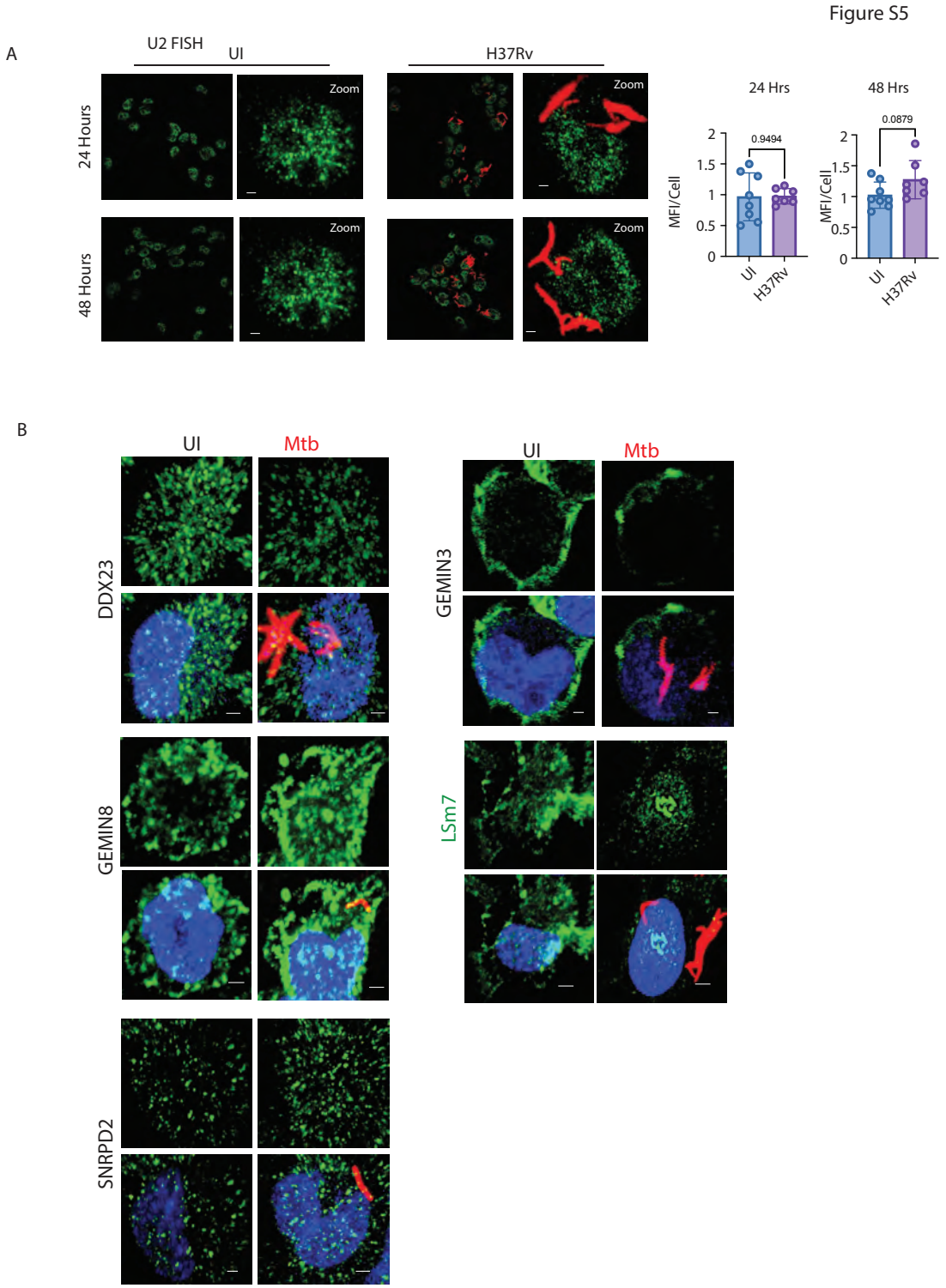

Figure S5: Dysregulation of splicing proteins upon Mtb infection.

A) Representative images for RNA FISH against U2 snRNA in THP-1 macrophages upon *Mtb* (mCherry-H37Rv) infection at 24- and 48-hrs post-infection. The U5 snRNA probe was labelled with Alexa 488 (green). Plots on the right show quantification of U2 snRNA FISH MFI in uninfected and *Mtb*-infected macrophages at 24 ad 48 hpi.

370 B) Representative image for staining of DDX23, GEMIN3, GEMIN8, LSm7 and
371 SNRPD2 in uninfected and H37Rv infected THP-1 macrophages 48 h post-
372 infection.
373
374

Figure S6

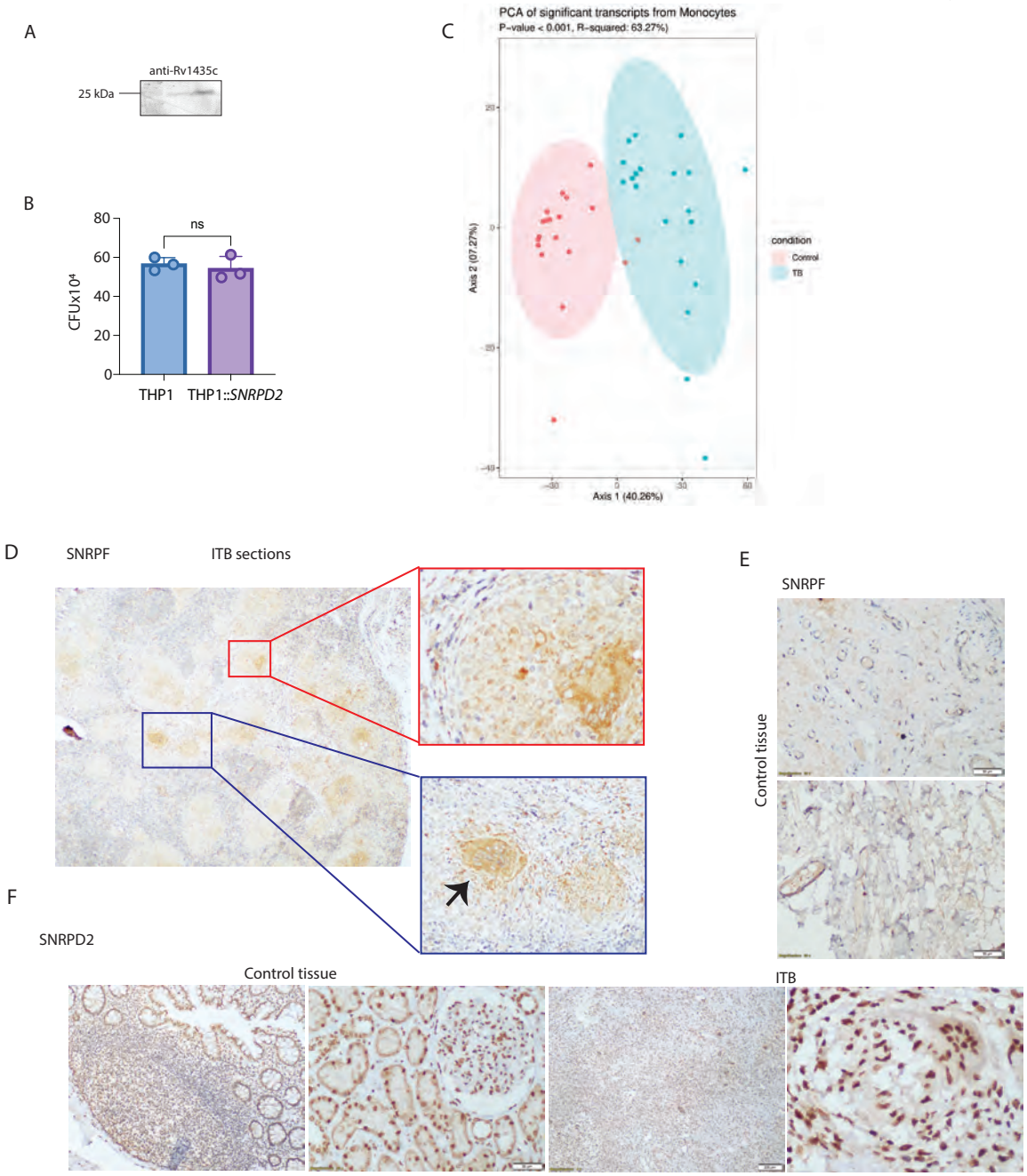

Figure S6: Regulation of host alternative splicing as a virulence mechanism

A) Western blot showing the specificity of anti-sera raised against Rv1435c.
B) The plot represents the bacterial CFU in WT THP-1 and THP-1::SNRPD2 at 48hr post-infection.
C) PCA analysis of significant transcripts (splice isoforms) identified by RNA-Seq in monocytes of Human TB patients.
D) Human intestinal tuberculosis granulomatous lesions were stained with SNRPF. Intense cytosolic staining in multinucleated giant cells (black arrow) is shown.
E) Representative image for IHC staining of SNRPF in gut sections from healthy controls.

F) Representative image for IHC staining of SNRPD2 in gut sections from healthy controls and in intestinal tuberculosis granulomatous lesions from diseased individuals.

Supplemental Tables:

Table S1: Spliceosome proteins identified in Y-12 pulldown MS analysis
Table S2: List of Mtb genes in the bait library (BD library) and human splicing factor coding transcripts in the prey library (AD library).
Table S3: List of genes included in the BD library as negative controls
Table S4: Yeast-2-hybrid interaction matrix for AD and BD proteins
Table S5: Two-column file for the interaction network shown in Fig 2B.
Table S6: RNAseq data shown in Fig. 8A.
Table S7: List of primers

Supplementary References

1 Liu, J. L. & Gall, J. G. U bodies are cytoplasmic structures that contain uridine-rich small nuclear ribonucleoproteins and associate with P bodies. *Proc Natl Acad Sci U S A* **104**, 11655-11659 (2007). https://doi.org/10.1073/pnas.0704977104

2 Bolger, A. M., Lohse, M. & Usadel, B. Trimmomatic: a flexible trimmer for Illumina sequence data. *Bioinformatics* **30**, 2114-2120 (2014). https://doi.org/10.1093/bioinformatics/btu170

3 Andrews, S. (2017).

4 Ewels, P., Magnusson, M., Lundin, S. & Kaller, M. MultiQC: summarize analysis results for multiple tools and samples in a single report. *Bioinformatics* **32**, 3047-3048 (2016). https://doi.org/10.1093/bioinformatics/btw354

5 Patro, R., Duggal, G., Love, M. I., Irizarry, R. A. & Kingsford, C. Salmon provides fast and bias-aware quantification of transcript expression. *Nat Methods* **14**, 417-419 (2017). https://doi.org/10.1038/nmeth.4197

6 Frankish, A. *et al.* GENCODE reference annotation for the human and mouse genomes. *Nucleic Acids Res* **47**, D766-D773 (2019). https://doi.org/10.1093/nar/gky955

7 Love, M. I. *et al.* Tximeta: Reference sequence checksums for provenance identification in RNA-seq. *PLoS Comput Biol* **16**, e1007664 (2020). https://doi.org/10.1371/journal.pcbi.1007664

8 Martin Morgan, V. O., Jim Hester, Hervé Pagès. SummarizedExperiment: SummarizedExperiment container. *R package version 1.28.0* (2022). https://doi.org/10.18129/B9.bioc.SummarizedExperiment

9 Zhu, A., Srivastava, A., Ibrahim, J. G., Patro, R. & Love, M. I. Nonparametric expression analysis using inferential replicate counts. *Nucleic Acids Res* **47**, e105 (2019). https://doi.org/10.1093/nar/gkz622

10 Vitting-Seerup, K. & Sandelin, A. IsoformSwitchAnalyzeR: analysis of changes in genome-wide patterns of alternative splicing and its functional consequences. *Bioinformatics* **35**, 4469-4471 (2019). https://doi.org/10.1093/bioinformatics/btz247

11 Kolde, R. Pheatmap: pretty heatmaps. *R package version v.1.0.12* (2019).

12 Chen, E. Y. *et al.* Enrichr: interactive and collaborative HTML5 gene list enrichment analysis tool. *BMC Bioinformatics* **14**, 128 (2013). https://doi.org/10.1186/1471-2105-14-128

13 Ashburner, M. *et al.* Gene ontology: tool for the unification of biology. The Gene Ontology Consortium. *Nat Genet* **25**, 25-29 (2000). https://doi.org/10.1038/75556

14 Wickham, H. ggplot2: Elegant Graphics for Data Analysis. *Springer-Verlag New York* (2016).

15 Team, R. C. R: A Language and Environment for Statistical Computing. (2022).

16 van Kessel, J. C. & Hatfull, G. F. Recombineering in Mycobacterium tuberculosis. *Nat Methods* **4**, 147-152 (2007). https://doi.org/10.1038/nmeth996

17 Xu, C. *et al.* Structural insights into Gemin5-guided selection of pre-snRNAs for snRNP assembly. *Genes Dev* **30**, 2376-2390 (2016). https://doi.org/10.1101/gad.288340.116